Quantum Time Crystals

Teddy Ong

Word Count (without appendices): 6853

Contents

1 Introduction

A conventional crystal, such as a diamond, is formed when a uniform collection of atoms spontaneously settles into a periodic structure upon cooling. Its continuous translation symmetry is broken and reduced to discrete translation symmetry. This can be detected by shining light on the crystal and observing its diffraction pattern.

Is it possible to create a "Time Crystal", a phase of matter where time translation symmetry can be broken? In this essay, we will define how symmetry breaking can be detected and highlight the desirable properties for such a phase as a *stable, macroscopic, conservative* "clock" [1]. We first examine continuous time translation symmetry and will see that it can be ruled out. The breakthrough comes in discrete time translation symmetry, manifested in driven systems. The notion of Many-Body Localisation (MBL) is demonstrated in the transverse field Ising model, then extended to a driven system. We will identify one of the phases to be a Discrete Time Crystal (DTC) and show that it is robust to several types of perturbation. Lastly, we examine recent experiments and whether they truly demonstrated MBL and DTC order.

1.1 Signatures of Symmetry Breaking

To diagnose symmetry breaking, we need to measure the dynamical signature of some well-chosen observable O. Here we restrict this to a local observable for experimental accessibility (in the topological setting however, this signature is only measurable in global logical operators but not local observables [2, 3]). The conventional definition for spatial translation symmetry breaking is as follows [4].

Definition: For a system in state $|\psi\rangle$, if there exists a local observable $O(\vec{x}, t)$ such that the correlation function converges to a non-zero function,

$$\lim_{|\vec{x}-\vec{x}'|\to\infty} \lim_{V\to\infty} \langle\psi| O(\vec{x}, 0)O(\vec{x}', 0) |\psi\rangle \to f(\vec{x} - \vec{x}') \neq 0 \tag{1}$$

a) then it has **spatial long-range order (LRO)** when f is a constant;
b) or **spatial crystalline order** when f is periodic.

For example, in the transverse field Ising model, the order parameter $O = Z_i$ is used to identify spatial LRO in the ground state (section 2.2.4). This definition inspires the following, which combines spatial long-range order and oscillations in time [4].

Definition: A system in state $|\psi\rangle$ displays **spatio-temporal order** if there exist a local observable $O(\vec{x}, t)$ such that the correlation function:

$$\lim_{|\vec{x}-\vec{x}'|\to\infty} \lim_{V\to\infty} \langle\psi| O(\vec{x}, t)O(\vec{x}', 0) |\psi\rangle \to f(t) \neq 0 \tag{2}$$

converges to a non-vanishing temporally periodic function $f(t)$.

A slightly different concept is spatial correlation, which represents the entanglement between sites that are far apart.

Definition: A state $|\psi\rangle$ is **short-range correlated** if *for all* local observables $O(\vec{x})$,

$$\lim_{|\vec{x}-\vec{x}'|\to\infty} \lim_{V\to\infty} \langle\psi| O(\vec{x})O(\vec{x}') |\psi\rangle - \langle\psi| O(\vec{x}) |\psi\rangle \langle\psi| O(\vec{x}') |\psi\rangle = 0 \tag{3}$$

otherwise, if there exist a local observable $O(\vec{x})$ such that the limit is non-zero or does not exist, then the state is **long-range correlated**.

For example, in a 1D chain of N spin 1/2's, product states $|\psi\rangle = \otimes_{i=1}^{N} |\phi_i\rangle$ are short-range correlated. This is because operators O_i, O_j localised on site i, j have exponentially small overlap when $\lim_{|i-j|\to\infty}$, therefore their action factorises:

$$\begin{aligned} O_iO_j |\psi\rangle &= |\phi_1\rangle \otimes ... \otimes O_i |\phi_i\rangle \otimes ... \otimes O_j |\phi_j\rangle \otimes ... \otimes |\phi_N\rangle \\ \langle\psi| O_iO_j |\psi\rangle &= \langle\phi_i| O_i |\phi_i\rangle \langle\phi_j| O_j |\phi\rangle_j) \\ &= \langle\psi| O_i |\psi\rangle \langle\psi| O_j |\psi\rangle \end{aligned} \tag{4}$$

On the other hand, "cat" states $|\pm\rangle = \frac{1}{\sqrt{2}} (|\uparrow\uparrow ... \uparrow\rangle \pm |\downarrow\downarrow ... \downarrow\rangle)$ are long-range correlated using the order parameter Z_i. This is because since $Z_i |\pm\rangle = |\mp\rangle$, therefore $\langle\pm| Z_iZ_j |\pm\rangle = 1$ while $\langle\pm| Z_i |\pm\rangle = 0$ by orthogonality $\langle\pm|\mp\rangle = 0$.

1.1.1 Local Operators

Since we utilise local operators for the above definitions, we will make precise the meaning of "local" and the compositions of such operators in a system of size L, using the definitions given in [5]. The support of an operator is the set of points on which it acts nontrivially. The diameter of a set is the supremum distance between any two points in the support.

Definition: An operator $O(\vec{x}, t)$ is **local** if its support has a finite diameter $\xi << L$ and is independent of system size.

Definition: An operator $A = \sum_i c_i A_i$ is **quasilocal** if it is the sum of operators A_i which are bounded and have coefficients $c_i \propto e^{-\alpha_i \text{diam}[\text{supp}(A_i)]}, \alpha_i > 0$ exponentially decaying with the diameter [5].

Definition: An operator U is a **local unitary** if it is can be approximated by a finite-depth quantum circuit composed of unitary gates whose maximum diameter l is finite and system-size independent, up to a difference exponentially decaying with l.

We note that many algorithms exist to implement the exponential of an anti-hermitian quasilocal operator A as a local unitary $V = e^{-A}$ [6, 7].

For a local operator O_j and a local unitary V, $VO_jV^\dagger$ is also a local operator. This is demonstrated in Fig 1, where for concreteness we represent $V = \prod_{i=1}^{2} \prod_j W_j^{(i)}$ as a two-layer circuit of local operators W of support $l = 5$, and O_j as a local operator of support $\xi = 4$.

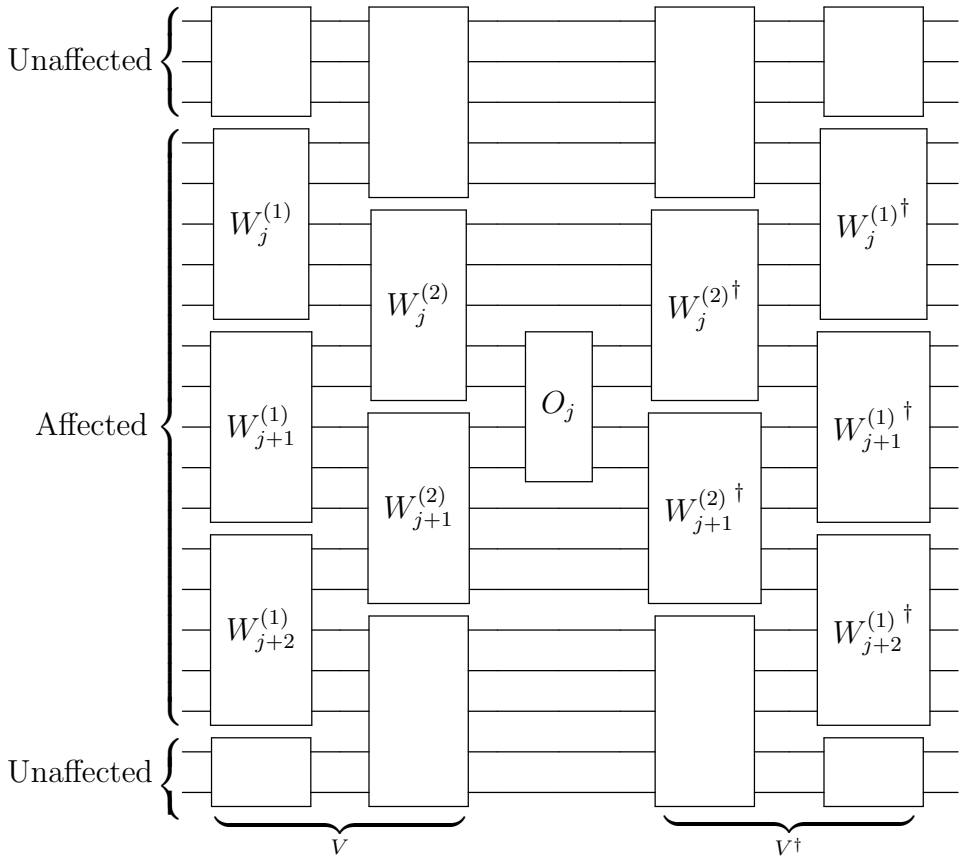

Figure 1: Under conjugation by a local unitary V, a local operator O_j with support ξ becomes $VO_jV^\dagger$ with support $\leq \xi + 4l$, which is still local as system size $L \to \infty$. Only a forward and backward "light cone" from O_j has any effect on qubits, whereas the gates without symbols will cancel out, leaving other qubits unaffected. Adapted from [5].

1.2 Desirable Properties of a Time Crystal

Eq 2 recognises that a collection of uncoupled simple harmonic oscillators, initialised *identically*, would display spatio-temporal order. However this order will be lost when local fields are perturbed, such that the oscillators' frequencies are shifted to generally incommensurate values. In that case, the limit $f(t)$ would have oscillation frequencies dependent on positions $\vec{x}, \vec{x}'$.

For a system with Hamiltonian H to be a *Time Crystal*, we require the following properties:

1. A large set of initial states (e.g. easily preparable product states) displays spatio-temporal order with the same observable $O(\vec{x}, t)$ and periodic function $f(t)$.

2. $f(t)$ is not changed when parameters are perturbed such that all other symmetries of H are removed.

These would imply that the phenomenon is not restricted to finely tuned points in parameter and initial state space, but rather a robust property intrinsic to time translation symmetry but not any other symmetries.

1.3 Continuous Time Translation Symmetry Breaking

The simplest setting to investigate is a time-independent Hamiltonian H, which has continuous time translation symmetry. An energy eigenstate $|\psi_n(t)\rangle$ with energy E_n evolves as $|\psi_n(t)\rangle = e^{-iE_nt/\hbar}|\psi_n(0)\rangle$. Is this breaking time-translation symmetry? No, because the phase factor will cancel out when measuring any observable O:

$$\langle\psi(t)|\,O\,|\psi(t)\rangle = \langle\psi(0)|\,e^{iEt/\hbar}Oe^{-iEt/\hbar}\,|\psi(0)\rangle = \langle\psi(0)|\,O\,|\psi(0)\rangle \tag{5}$$

1.3.1 AC Josephson Effect

The AC Josephson effect is a well-known example of oscillatory behaviour under static conditions using superconductors. Superconductors have ground states that are characterised by the formation of Cooper pairs - pairs of electrons of opposite spin and momentum $\boldsymbol{k}$. The ground state can be written in the following form [8, 9]:

$$|\psi_\phi\rangle = \prod_{\boldsymbol{k}}(u_{\boldsymbol{k}} + v_{\boldsymbol{k}}e^{i\phi}c^\dagger_{\boldsymbol{k}\uparrow}c^\dagger_{-\boldsymbol{k}\downarrow})\,|0\rangle \tag{6}$$

where $c^\dagger, c$ are creation and annihilation operators. Coefficients $u_{\boldsymbol{k}}, v_{\boldsymbol{k}}$ are chosen to be real and ϕ is an arbitrary phase, also called the superconducting phase.

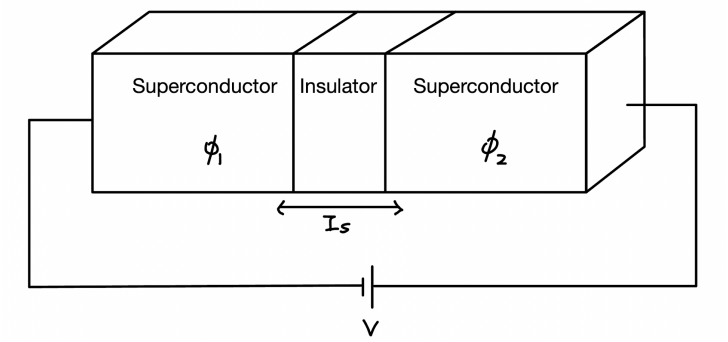

Figure 2: Two superconductors with phases ϕ_1, ϕ_2 are separated by an insulator. An external voltage V is applied and a current I_s is induced due to electrons tunnelling through the barrier.

Two superconductors are separated by an insulator which allows electrons to tunnel through the barrier (Fig 2). When a voltage applied across the Josephson junction, an oscillating supercurrent I_s is induced. The system is governed by the following Hamiltonian ([10, pp. 5–6]):

$$H = -E_J\cos\phi + 2eVn + \frac{n^2}{2C} \tag{7}$$

where $\phi = \phi_1 - \phi_2$ is the superconducting phase difference, which is conjugate to the Cooper pair number n; E_J is the Josephson energy for the tunnelling of a pair across the junction, C is the junction capacitance, and V is the voltage difference across the junction. When $E_J << \frac{e^2}{2C}$, H has an approximate internal U(1) phase symmetry for ϕ where $\dot{\phi} = 2eV + \frac{n}{C}$ remains constant. This leads to a supercurrent $I_s = \dot{n} = E_j\sin\phi$

with oscillation period $T = \frac{2\pi}{\dot{\phi}}$.

This is an example of time translation symmetry breaking that "piggybacks" on the spontaneous U(1) symmetry breaking of ϕ. It is also not stable to arbitrary time-translation symmetry-respecting perturbations; a perturbation that breaks the "primary" symmetry will cause the oscillations to decay [11, p. 27]. The capacitance term causes the system to behave like a non-linear oscillator with dephasing time $\tau = \sqrt{C/E_J}$ [10]. For these reasons, the AC Josephson effect is not considered a Time Crystal.

1.3.2 No-Go Theorem

If we had an isolated system which was a time crystal, we would expect its ground state to display spatio-temporal order as a combination of time translation symmetry breaking and spatial uniformity. For example, the ground state of the classical Ising model $H = -\sum_i J_i Z_i Z_{i+1} - h_i Z_i$ is $|\uparrow ... \uparrow\rangle$, which exhibits this spatial uniformity. However, this would not be possible due to the following theorem and corollary by Wantanabe and Oshikawa [4].

Theorem 1: For an isolated system under a time-independent local hamiltonian H, let *Integrated Observables* $A(t) \equiv \sum a(\vec{x}, t)$, $B(t) \equiv \sum b(\vec{x}, t)$ be the sums of local observables $a(\vec{x}, t), b(\vec{x}, t)$. Then

$$\left| \frac{1}{V^2} \langle 0| A(t)B(0) |0\rangle - \langle 0| A(0)B(0) |0\rangle \right| \leq C\frac{t}{V} \tag{8}$$

and hence that taking the limit $V \to \infty$ forces $\langle 0| \frac{A(t)}{V} \frac{B(0)}{V} |0\rangle = 0$. Hence spatially averaged observables cannot show spatio-temporal order. (Proof in Appendix A.)

Corollary 1.1: No state $|\psi\rangle$ can have spatio-temporal order.

> **Proof**: Assuming a system in state $|\psi\rangle$ showed spatio-temporal order for observables $a(\vec{x}, t), b(\vec{x}, t)$. Note that this is more general than Eq 2 in which $a = b = O$.
>
> $$\lim_{|\vec{x}-\vec{x}'|\to\infty} \lim_{V\to\infty} \langle \psi| a(\vec{x}, t)b(\vec{x}', 0) |\psi\rangle \to f(t) \tag{9}$$
>
> Then the spatially-averaged observables also display spatio-temporal order,
>
> $$\lim_{V\to\infty} \frac{1}{V^2} \langle 0| A(t)B(0) |0\rangle = \lim_{V\to\infty} \frac{1}{V^2} \sum_{\vec{x}} \sum_{\vec{x}'} \langle 0| a(\vec{x}, t)b(\vec{x}', 0) |0\rangle \sim f(t) \tag{10}$$
>
> since this sum is dominated by terms with large separation $\vec{x} - \vec{x}'$. However this contradicts theorem 1, thus no state $|\psi\rangle$ can have spatio-temporal order.

1.4 Discrete Time Translation Symmetry Breaking

Having shown that spatio-temporal order is not possible in an isolated system, we investigate whether it might be possible to break a reduced symmetry - discrete instead of continuous time translation. In a driven system with hamiltonian $H(t+T) = H(t)$ of period T, break this discrete symmetry means a *subharmonic* response: a dynamical signature has period $T' = nT$ for some integer $n > 1$. Classical examples include Faraday Waves, where a container of water with a liquid-air interface is shaken vertically at frequency ω_D, surface waves develop that oscillate at frequencies $\omega = \frac{n}{m}\omega_D$, which are rational subharmonics of the drive [10]. However these depend on dissipative effects. Experimentally, open systems with dissipation have been shown to break even continuous time translation symmetry [12]. We aim to find a driven system that does not rely on dissipation to exhibit subharmonic response.

1.4.1 Floquet Systems

A periodically driven system is also known as a Floquet system. Without continuous time translation symmetry, energy is not conserved. Through the following definitions, we establish the concept of "quasienergy" in driven systems.

Definition: For the one-period time-evolution Floquet unitary U_F, where $|\phi(t+T)\rangle = U_F |\phi(t)\rangle$, the **Floquet Hamiltonian** H_F is a time-independent operator defined formally as [13]:

$$U_F = T \exp\left[-\frac{i}{\hbar}\int_0^T H(\tau)d\tau\right] \equiv \exp\left[-\frac{i}{\hbar}H_F T\right] \tag{11}$$

where $T\exp$ is the time-ordered exponential. Since U_F is unitary, it has eigenstates with eigenvalues of modulus 1. Examples of how to manually calculate H_F can be found in [14]. For convenience, we set $\hbar = 1$.

Definition: The **quasienergy** ϵ_ψ of an eigenstate $|\psi(t)\rangle$ of the Floquet unitary U_F is such that $U_F |\psi(t)\rangle = e^{-i\epsilon_\psi T} |\psi(t)\rangle$. Correspondingly, $H_F |\psi(t)\rangle = \epsilon_\psi |\psi(t)\rangle$ (modulo $\frac{2\pi}{T}$).

1.4.2 Conditions for DTTSB

The following result [15] will be crucial in diagnosing whether discrete time translation symmetry breaking (DTTSB) can occur by examining eigenstates of U_F.

Theorem 2: The following definitions are equivalent:

1. DTTSB occurs if for all time t and for all short-ranged correlated state $|\alpha(t)\rangle$, there exists a local operator O such that $\langle\alpha(t+T)| O |\alpha(t+T)\rangle \neq \langle\alpha(t)| O |\alpha(t)\rangle$.

2. DTTSB occurs if the eigenstates of the Floquet unitary U_F cannot be short-range correlated and if the eigenspectrum of U_F is non-degenerate.

Proof:
$1 \Rightarrow 2$: A Floquet eigenstate with $U_F \left|\psi(t)\right\rangle = e^{-i\epsilon_\psi T} \left|\psi(t)\right\rangle$ must satisfy:

$$\left\langle\psi(t+T)\right| O \left|\psi(t+T)\right\rangle = \left\langle\psi(t)\right| e^{+i\epsilon_\psi T} O e^{-i\epsilon_\psi T} \left|\psi(t)\right\rangle = \left\langle\psi(t)\right| O \left|\psi(t)\right\rangle \quad (12)$$

This violates the first clause if $\left|\psi(t)\right\rangle$ is short-range correlated.

$1 \Leftarrow 2$: If all eigenstates are long-range correlated, then a short-range correlated state $\left|\alpha(t)\right\rangle$ must be superpositions of different Floquet eigenstates: $\left|\alpha(t)\right\rangle = \sum_\psi a_\psi \left|\psi(t)\right\rangle$. Then $\left|\alpha(t+T)\right\rangle = \sum_\psi a_\psi e^{-i\epsilon_\psi T} \left|\psi(t)\right\rangle$.

$$\left\langle\alpha(t+T)\right| O \left|\alpha(t+T)\right\rangle = \sum_{\psi_1}\sum_{\psi_2} a^*_{\psi_1} a_{\psi_2} e^{-i(\epsilon_{\psi_2}-\epsilon_{\psi_1})T} \left\langle\psi_1(t)\right| O \left|\psi_1(t)\right\rangle \quad (13)$$

We can see that this will not be equal to $\left\langle\alpha(t)\right| O \left|\alpha(t)\right\rangle$ due to the distinct eigenvalues $\epsilon_{\phi_1} \neq \epsilon_{\phi_2}$ within the composition of $\left|\psi(t)\right\rangle$.

Remark: The first definition is easily probed in experiments - prepare a system in a product state and observe its subsequent time-evolution. The second definition is easier to probe in theory and numerical simulation.

2 Theoretical Discussion

So far we have established that in order to look for DTTSB, we want to find a driven system whose Floquet eigenstates are long-range correlated with non-degenerate quasienergy pectrum.

However, a driven system without any means of dissipation is generally expected to absorb energy and thermalise. One possibility is for the drive frequency to be much larger than the local bandwidth, so that the system cannot effectively absorb one quantum of energy in the form of a spin- / domain wall-flip. However this will still cause thermalisation with exponentially long time.

Even in an isolated system where unitary evolution preserves all information about the initial state, the **Eigenstate Thermalisation Hypothesis (ETH)** proposed by Deutsch [16] and Srednicki [17] states that eigenstate expectation values agree with thermodynamic ensemble averages at the temperature associated with the energy density of the eigenstate [18]. Therefore not only is a thermal system unable to display DTTSB, one will not be able to distinguish between different eigenstates at large times (Appendix B). In order to prevent this from happening, we turn to a phenomenon called Many-Body Localisation.

2.1 Many-Body Localisation in an Isolated System

Many-Body Localisation (MBL) is a phenomenon where an isolated system never reaches local thermal equilibrium. Instead expectation values of local operators equilibrate to a steady-state value that does not agree with the thermodynamic ensemble average.

To examine how MBL can be produced, we consider the Transverse Field Ising Model (TFIM) on a 1D chain of N spin 1/2's [1, p. 18]:

$$\begin{aligned} H &= H_0 + \delta H \\ H_0 &= -\sum_{i=1}^{N-1} J_i Z_i Z_{i+1} \\ \delta H &= -\sum_{i=1}^{N} h_i^x X_i \end{aligned} \tag{14}$$

In the limit $h_i^x = 0$, both the N single-site magnetisations Z_i and the $N-1$ domain walls $D_i = Z_i Z_{i+1}$ commute with H_0 and thus are preserved at all times. Note that Eq 14 possesses a $\mathbb{Z}_2$ *Ising Symmetry* generated by $P_x = \prod_i X_i$ even under perturbation δH. We choose to identify D_i as **physical bits** ("p-bits") of the system as they commute with P_x, whereas Z_i do not. The eigenstates are fully determined by the eigenvalues d_i, p_x under D_i, P_x.

E.g. $|\boldsymbol{d}_\pm\rangle \equiv |\{d_1 = +1, d_2 = -1, d_3 = +1\}, p_x = \pm 1\rangle = \frac{1}{\sqrt{2}}\left(|\uparrow\uparrow\downarrow\downarrow\rangle \pm |\downarrow\downarrow\uparrow\uparrow\rangle\right)$.

MBL refers to the persistence of preserved local quantities in the presence of perturbation h_i^x when we have sufficiently large disorder, achieved by drawing J_i

independently and identically distributed (i.i.d.) from a distribution with standard deviation W. In this case, the objects preserved are $N-1$ **logical bits** ("l-bits") I_i that satisfy the following conditions [19]:

1. They commute with each other and the Hamiltonian. $[I_i, I_j] = [H, I_i] = 0 \ \forall i, j$

2. They are binary ($I_i^2 = 1$), functionally independent and complete, such that each of 2^N eigenstates can be labelled by a unique set of eigenvalues of I_i together with the Ising symmetry P_x.

3. They are related to p-bits by a *local unitary* V (in this case $I_i = VD_iV^\dagger$). The new eigenstates are related to the eigenstates of the unperturbed Hamiltonian by $|\tilde{\psi}\rangle = V|\psi\rangle$.

4. The Hamiltonian can be expressed in the following form [20]:

$$H_{MBL} = B_0 + \sum_i B_i I_i + \sum_{i,j} K_{ij} I_i I_j + \sum_{i,j,k} K_{ijk} I_i I_j I_k + ... \tag{15}$$

where the couplings K_{ij} decay exponentially in distance $|i-j|$. $|B_i|$ is on the order of the typical *local bandwidth* (energy separation between eigenstates with one l-bit flipped). This is referred to as *emergent integrability*. As a result, $\dot{I}_i = \frac{i}{\hbar}[H, I_i] = 0$. Note that in literature, MBL usually refers to N l-bits, however here we partition the system into two sectors of $N-1$ l-bits to highlight the Ising symmetry and domain wall dynamics (section 2.1.2).

We prove in Appendix C that any system always has operators that satisfy only condition 1 and 2, but they may be highly non-local. Without MBL, quantum information is spread over experimentally inaccessible degrees of freedom.

When cast into this form, the MBL system behaves like a system of weakly coupled pseudo-spins S, with $I_i \equiv S_i^z$ being the z-component of these spins. [20] showed that corresponding x and y spin components S_i^x, S_i^y can be constructed in a way that, together with S_i^z, behave in the same way as Pauli operators. The spins' xy components precess around the z-axis at a rate depends on all other I_i due to the interactions. Thus the xy components are entangled with the z components of other spins, leading to dephasing dynamics which causes to the entanglement to only grow logarithmically in time [21]. This is in contrast to thermalising systems, where this growth is ballistic in time given by the Lieb-Robinson bound [22]. The consequence is that the the system looks thermal when measuring $\langle S_i^x(t))\rangle$ but static for $\langle S_i^z(t))\rangle$.

2.1.1 Quasilocality

Imbrie [23] showed that one can construct a sequence of local unitary (section 1.1.1) operators that diagonalise the Hamiltonian, from which the l-bits arise as the binary encoding of the new basis states (Appendix C). We summarise the core argument and apply it to our case where Ising symmetry P_x is preserved.

First, we may write the unperturbed Hamiltonian $H_0 = -\sum_i J_i D_i$, whose eigenstates $|\boldsymbol{d}_\pm\rangle$ have energies $E(\boldsymbol{d}) = -\sum J_i d_i$. Let $|\boldsymbol{d}_\pm^{(i)}\rangle = X_i |\boldsymbol{d}_\pm\rangle$ be the eigenstate which differs by a spin flip at position i. This causes a change in energy $\Delta E(\boldsymbol{d}, i)$,

$$\Delta E(\boldsymbol{d}, i) \equiv E(\boldsymbol{d}) - E(\boldsymbol{d}^{(i)}) = 2(J_{i-1}d_{i-1} + J_i d_i) \tag{16}$$

which we assume to be much larger than the size of the perturbation h_i^x. Let the operator $A = \sum_i A_i$, where the only matrix elements of A_i in this basis is between states which differ by a single flip at spin i:

$$A_i |\boldsymbol{d}_\pm\rangle = \frac{h_i^x}{E(\boldsymbol{d}) - E(\boldsymbol{d}^{(i)})} |\boldsymbol{d}_\pm^{(i)}\rangle \tag{17}$$

Since $\Delta E(\sigma, i)$ only depends on the values of spins d_{i-1}, d_i, d_{i+1}, A_i is a local operator, which makes A quasilocal. Furthermore, A_i is an antisymmetric real matrix, hence $V = e^{-A}$ is a *local unitary*. Next we observe the effect of $[A, H_0]$ in this basis:

$$\begin{aligned} [A, H_0] |\boldsymbol{d}_\pm\rangle &= AE(\sigma) |\boldsymbol{d}_\pm\rangle - H_0 \frac{h_i^x}{\Delta E(\boldsymbol{d}, i)} |\boldsymbol{d}_\pm^{(i)}\rangle \\ &= h_i^x |\boldsymbol{d}_\pm^{(i)}\rangle \\ [A, H_0] &\equiv \sum_i h_i^x X_i \end{aligned} \tag{18}$$

To first order, we can then remove the perturbation from $H = H_0 + \delta H$ using V to change frames,

$$\begin{aligned} \tilde{H} &= e^A H e^{-A} \\ &= H + [A, H] + ... \\ &= (H_0 + \delta H) - (\delta H + [A, \delta H]) + ... = H_0 + ... \end{aligned} \tag{19}$$

where the ... represents higher order terms, which can be removed inductively order-by-order [23]. This means that eventually, $H = V H_0 V^\dagger$, yielding the $N - 1$ l-bits $I_i = V D_i V^\dagger$.

Next, we demonstrate why disorder in the couplings J_i is also needed to produce MBL. We will see that with uniform couplings, domain walls D_i can propagate freely, forming "plane-wave" eigenstates, whereas disorder stops this and produces localisation.

2.1.2 Uniform Couplings - Domain Wall Propagation

When all couplings J_i are equal, the energy cost of a domain wall (where two neighbouring spins are anti-aligned) is independent of location, and so domain walls can propagate freely. They do so when the perturbation hX_i flips a spin adjacent to the domain wall. This is most clearly illustrated dynamically by looking at the time-evolution unitary for a discrete duration $t = \frac{2\pi}{4J}$ and in the interaction picture of $H_z = -\sum_i JZ_iZ_{i+1}$. Subrahmanyam [24] showed that the time evolution operator becomes (full details in Appendix D):

$$U\left(t = \frac{2\pi}{4J}\right) = \prod_i \left[\cos\left(\frac{\pi h}{4J}\right) - i\sin\left(\frac{\pi h}{4J}\right) X_i\left(1 - Z_{i-1}Z_{i+1}\right)\right] \tag{20}$$

We see that when applied onto a product state $|\uparrow \ldots \downarrow\rangle$ (which is not an eigenstate of the perturbed hamiltonian), the operator $X_i\left(1 - Z_{i-1}Z_{i+1}\right)$ will flip the spin at site i if the spins at site $i-1, i+1$ are anti-aligned, and is zero otherwise. Therefore, this unitary operator only propagates domain walls either left or right, but cannot create or destroy them.

The presence of these "delocalised" domain walls destroys the long-range correlation between spins. The above time evolution causes the system to thermalise, as initial local information (domain walls) become spread out throughout the system.

2.1.3 Disordered Couplings - Localisation

If the signs of J_j are random, then in $\geq$2D it becomes impossible to satisfy all the interactions in an energetically favourable way, creating the phenomenon of *frustration*. This leads to situations where more than one arrangement of spins is stable.

In 1D, When J_i are drawn randomly from a distribution, neighbouring values are generally distinct $J_i \neq J_{i+1}$, hence domain walls cannot propagate as it will incur energy costs. Therefore at low temperatures, domain walls tend to be localised where J_i values are small. States of similar energy would have very different configurations of domain walls, making them inaccessible through unitary evolution. Therefore the phenomenon of *localisation* is produced, where domain walls and hence individual spins are frozen in place.

The eigenstates of Eq 14 are termed **Spin-Glass** states, as remain approximately of the form $\approx \frac{1}{\sqrt{2}}\left(|\uparrow\downarrow \ldots \uparrow\rangle \pm |\downarrow\uparrow \ldots \downarrow\rangle\right)$ under perturbation.

Upon adding more interaction terms, such as $H_{int} = \sum_i J_{int}(Z_iZ_{i+2} + X_iX_{i+2})$, localisation may be overcome and the system once again thermalises [1, p. 19].

2.2 MBL in a Driven System

Having shown that MBL could exist in an isolated system, we now seek DTTSB. Consider a 1D chain of N spin 1/2's driven with period $T = 1$. The system is evolved under the following hamiltonian for times T_1, T_2, T_3 respectively with $T_1 + T_2 + T_3 = T$.

$$H \equiv \begin{cases} H_1 & = \mathfrak{g} \sum_{i=1}^{N} X_i \\ H_2 & = -\sum_{i=1}^{N-1} \mathfrak{J}_i Z_i Z_{i+1} - \sum_{i=1}^{N} \mathfrak{h}_i^z Z_i \\ H_3 & = -\sum_{i=1}^{N} \mathfrak{h}_i^x X_i \end{cases} \tag{21}$$

Here we fix the driving duration and vary $\mathfrak{g}, \mathfrak{J}_i, \mathfrak{h}_i^{z,x}$ to achieve the desired effective couplings $g = \mathfrak{g}T_1, J_i = \mathfrak{J}_i T_2, h_i^z = \mathfrak{h}_i^z T_2, h_i^x = \mathfrak{h}_i^x T_3$. However, experimentally it may be easier to vary the durations T_1, T_2, T_3 instead. The Floquet unitary is given by:

$$U_F \equiv \exp\left[i \sum h_i^x X_i\right] \exp\left[i \sum_i \left(J_i Z_i Z_{i+1} + h_i^z Z_i\right)\right] \exp\left[-ig \sum_i X_i\right] \tag{22}$$

Here we view $h_i^{x,z}$ as small perturbations and set them to zero for initial discussion. Let $\bar{J} = \frac{1}{N}\sum_i J_i$ be the average coupling strength, where J_i are drawn i.i.d. from some distribution. The drive also possesses the *Ising Symmetry* $P_x = \prod_i X_i$, a global spin flip. Note that when $g = \pi/2$, the first term becomes:

$$\exp\left[-ig \sum_i X_i\right] = \prod_i \left(\cos(g)\mathbb{1}_i - i\sin(g)X_i\right) = (-i)^N \prod_i X_i \propto P_x \tag{23}$$

We neglect the global phase factor $(-i)^N$ as it will not affect any dynamical signatures. U_F is a local unitary, as it can be represented as a finite-depth quantum circuit composed of local operators (Fig 3).

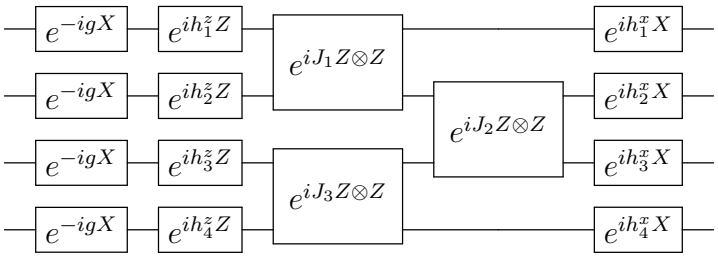

Figure 3: Representation of U_F as a quantum circuit on $N = 4$ qubits. $\exp[-igX_i]$ is applied to each qubit, followed by $\exp[ih_i^z Z_i]$. $\exp[i\sum_i J_i Z_i Z_{i+1}]$ is executing using two layers of disjoint two-qubit gates $e^{iJ_i Z_i Z_{i+1}}$. Finally, $\exp[ih_i^x X_i]$ is applied to each qubit.

2.2.1 Dimensionality and Long-ranged Interaction

Here we examine 1 dimensional, nearest-neighbour couplings, although in many experiments there would be long-ranged interactions of the form $\sum_{i,j} \frac{J_{ij}}{r^\alpha} Z_i Z_j$ due to Coulomb or dipole-dipole interactions. However, MBL is destabilised by spin-spin resonances [25] when $\alpha < d$, two-spin pairwise resonance when $\alpha < 2d$, and by Ergodic Grains [26] when $d \geq 2$. Hence we require $d = 1, \alpha > 2$ for MBL to be possible. Further discussion can be found in Appendix E.

2.2.2 Paramagnet (PM) Phase

When $J_i = 0, g > 0$, the Floquet eigenstates are product states of $|\rightarrow\rangle$ or $|\leftarrow\rangle$, the eigenstates of X_i, with randomly distributed quasienergies (Fig 4a). Since all eigenstates are short-range correlated, we cannot have DTTSB.

2.2.3 0π Paramagnet Phase

When $J_i = \pi/2, g > 0$, $\exp\left[-i\sum_{i=1}^{N-1} J_i Z_i Z_{i+1}\right] = (-i)^{N-1} Z_1 Z_L$. This phase of matter is a bulk paramagnet which exhibits DTTSB on the boundary [1, 13]. This is beyond the scope of this essay.

2.2.4 0 Spin Glass (0SG) Phase

When $J_i > 0, g = 0$, this is exactly the undriven case discussed in section 2.1. The ground state is $|0_\pm\rangle = \frac{1}{\sqrt{2}}(|\uparrow \ldots \uparrow\rangle \pm |\downarrow \ldots \downarrow\rangle)$. The perturbed ground state $|\tilde{0}_\pm\rangle$ remain degenerate up to a difference exponentially small in system size, $(h/J)^N$. With an order parameter Z_j, it displays spatial long-range order as defined in Eq 1 [1, p. 19].

$$\lim_{L\to\infty} \langle\tilde{0}_\pm| Z_i Z_j |\tilde{0}_\pm\rangle \neq 0 \tag{24}$$

All eigenstates of either parity $|\boldsymbol{d}_\pm\rangle$ have the same quasienergy $\epsilon = -\sum J_i d_i$. Therefore the entire quasienergy spectrum is paired and degenerate, but randomly distributed within any parity sector $p_x = \pm 1$ (Fig 4b). This degeneracy means that any product state does not display DTTSB (Theorem 2).

2.2.5 π Spin Glass (πSG) Phase

When $J_i > 0, g = \pi/2$, the Floquet eigenstates the same as above. The key difference is that the two eigenstates now have different eigenvalues under U_F, since $U_F |\boldsymbol{d}_\pm\rangle = \pm e^{i\sum J_i d_i}$. The factor of $-1 = e^{-i\pi}$ leads to a difference of π for their quasienergies, hence the name of the phase. The entire quasienergy spectrum is paired with gap π, and randomly distributed within any parity sector $p_x = \pm 1$ (Fig 4c). Hence in general it is not degenerate and DTTSB is possible. The distribution of quasienergy spectrum is summarised in Fig 4. A circle is used since quasienergies are defined modulo $2\pi/T$.

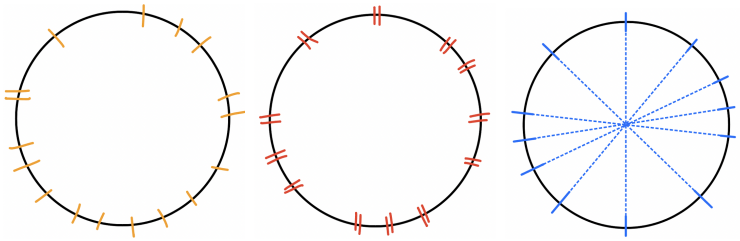

(a) PM (b) 0SG (c) πSG

Figure 4: (a) In the PM phase, they are randomly distributed. (b) In the 0SG phase, they are randomly distributed but pairwise degenerate. (c) In the πSG phase, each pair is randomly distributed with π difference.

If we start with a symmetry-broken state $|\uparrow\downarrow \ldots \uparrow\rangle$, it will be preserved by $e^{-iH_2T_2}$ and flipped by P_x. Unsurprisingly it exhibits *period-doubled dynamics*, where it returns to its initial state in time $2T$ rather than T. This subharmonic response is a particular example of DTTSB corresponding to cycling through $\mathbb{Z}_2$ Ising symmetry. This can be extended to other finite groups such as $\mathbb{Z}_n, Q_8$, etc [27]. We aim to show that this phenomenon persists under generic perturbations and for any symmetry-broken initial state.

2.2.6 Phase Diagram

Operators of the form $\exp(-igX_j)$ are periodic in g with period π. Hence we may restrict our attention to the region $g, \bar{J} \in [0, \pi/2]$. We may then conjecture the phase diagram as follows:

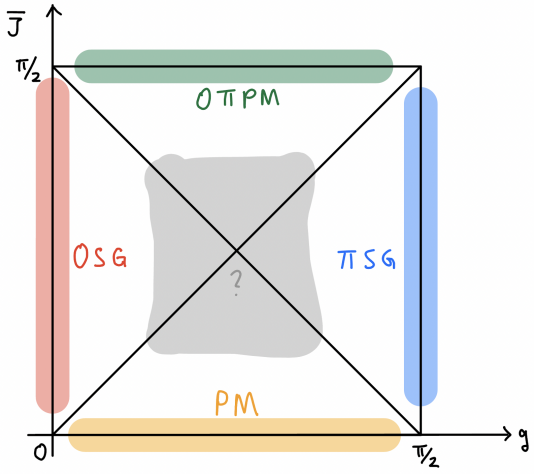

(a) Phase Diagram

Figure 5: Phase diagram of driven Ising model.

Here we make a key assumption: the parameter values discussed above used to identify the phases are in the *interior* of the phase, such that perturbation theory is valid up to some extent away from the exactly solvable lines (coloured area). However, it is not clear what lies in between these lines (grey area). [28, p. 11] suggests that a thermal phase lies between the PM and πSG phases.

2.3 Absolute Stability

The πSG phase (section 2.2.5) is a good candidate for MBL and DTTSB as it has disordered couplings, long-range correlated eigenstates $|\psi\rangle$, and a non-degenerate quasienergy spectrum. We now assume that MBL, which was discussed in the un-driven setting (0SG) persists under the drive $g = \pi/2$ in the πSG phase. The domain walls $D_i = Z_i Z_{i+1}$, which commute with P_x and thus the unperturbed Floquet unitary U_F, act as p-bits.

Under some perturbations, let $|\tilde{\psi}\rangle$ be the new eigenstates of the perturbed Floquet unitary $\tilde{U}_F$. Under the assumption of MBL, there exist a local unitary V such that $|\tilde{\psi}\rangle = V|\psi\rangle$. We can construct the **logical bits** $\tilde{D}_i = VD_iV^\dagger$ and an **emergent Ising symmetry** $\tilde{P}_x = VP_xV^\dagger$. Since V is a local unitary, $\tilde{D}_i$ is still exponentially localised.

The eigenvalues of $\tilde{D}_i, \tilde{P}_x$ with respect to $|\tilde{\psi}\rangle$ are the same as those of D_i, P_x for $|\psi\rangle$, therefore their matrix representations are identical. Therefore they commute with $\tilde{U}_F$ as they are diagonal in the new eigenstate basis. Eigenstates are "cat" states of the emergent Ising symmetry, $|\{\tilde{d}_i\}, \tilde{p}_x = \pm 1\rangle$ and remain long-range correlated.

Define $\tilde{\tau}_i = VZ_iV^\dagger$ such that $\tilde{D}_i = \tilde{\tau}_i\tilde{\tau}_{i+1}$. Note that $\tilde{P}_x$ commutes with $\tilde{D}_i$ but anti-commutes with $\tilde{\tau}_i$. Von Keyserlingk [29] showed the following theorem, which will allow us to conclude that the form of $\tilde{U}_F$ can be written as Eq 28.

Theorem 3: $\tilde{U}_F$ and $\tilde{\tau}_i$ remains anti-commuting under perturbations, under continuity assumptions.

Proof: $\forall r, s$, $\tilde{\tau}_r\tilde{\tau}_s = \prod_{i=r}^{s-1} \tilde{D}_i$. This commutes with $\tilde{U}_F$ since $\tilde{D}_i$ do. Now consider:

$$\begin{aligned} \theta_r &\equiv \tilde{\tau}_r\tilde{U}_F^\dagger\tilde{\tau}_r\tilde{U}_F \\ \theta_s &\equiv \tilde{\tau}_s\tilde{U}_F^\dagger\tilde{\tau}_s\tilde{U}_F \end{aligned} \tag{25}$$

The motivation is that $\langle\tilde{\psi}|\,\theta_r\,|\tilde{\psi}\rangle = \langle\tilde{\psi}|\,\tilde{\tau}_r(0)\tilde{\tau}_r(T)\,|\tilde{\psi}\rangle$ is the unequal time autocorrelator at site r. $\tilde{U}_F$ is represented by a finite-depth local unitary quantum circuit (section 2.2). Therefore θ_r, θ_s are also local operators.

$$\begin{aligned} \tilde{\tau}_r\tilde{\tau}_s &= \tilde{U}_F^\dagger\tilde{\tau}_r\tilde{\tau}_s\tilde{U}_F \\ &= \tilde{\tau}_r\theta_r\theta_s^\dagger\tilde{\tau}_s \end{aligned} \tag{26}$$

where we used the fact that $\tilde{\tau}_s^2 = \mathbb{1}$. Therefore $\theta_r = \theta_s$. However, they are exponentially localised about r, s. Therefore as $|r - s| \to \infty$, we must have $\theta_r = \theta_s \in \mathbb{C}$, as they cannot possible contain any shared operators. Then,

$$\begin{aligned} \tilde{\tau}_r\theta_r &= \tilde{U}_F^\dagger\tilde{\tau}_r\tilde{U}_F \\ \tilde{\tau}_r^2\theta_r^2 &= \tilde{U}_F^\dagger\tilde{\tau}_r\tilde{U}_F\tilde{U}_F^\dagger\tilde{\tau}_r\tilde{U}_F \\ \theta_r^2 &= 1 \end{aligned} \tag{27}$$

in which we squared the first line, and $\tilde{\tau}_r\theta_r = \theta_r\tilde{\tau}_r$ since $\theta_r \in \mathbb{C}$. Thus $\theta_r = \pm 1$. Given that in the unperturbed case, $\theta_r = -1$, and assuming that $V, \tilde{U}_F$ is a continuous family of unitaries and assuming continuity, $\theta_r = -1$ will persist under perturbation.

Based on the above commutation relations, we know that $\tilde{P}_x$ must persist in $\tilde{U}_F$ since it is needed to produce the anti-commuting property with $\tilde{\tau}_r$. We may now write:

$$\tilde{U}_F = \exp\left[-iH_{MBL}(\tilde{D}_i)\right]\tilde{P}_x \tag{28}$$

Where H_{MBL} is of the form Eq 15. Note that U_F and $\tilde{U}_F$ are not related by V, since they generally have different spectrum of eigenvalues.

Since the Floquet unitary $\tilde{U}_F$ retains the same form, it will also exhibit MBL with the new l-bits $\tilde{D}_i$. We call an operator "Ising-even" if it commutes with $\tilde{P}_x$, and "Ising-odd" if it anti-commutes. For example, any product of an even number of $\tilde{\tau}_i$, including $\tilde{D}_i$, are Ising-even and thus are preserved under $\tilde{U}_F$. A product of an odd number of $\tilde{\tau}_i$ is Ising-odd and is flipped by unitary evolution: $\tilde{\tau}_i(nT) = (-1)^n\tilde{\tau}_i$.

Now we explicitly demonstrate the stability of πSG under certain kinds of perturbations [1, pp. 39,45].

2.3.1 Symmetry-Preserving Perturbation

For $g = \frac{\pi-\epsilon}{2}, \epsilon > 0, h_i^z = 0$, we have an imperfect Ising flip with Ising symmetry P_x preserved, i.e. P_x commutes with H_2, H_3. Therefore by considering the Floquet unitary for two periods, we see that P_x cancels out.

$$\begin{aligned}\tilde{U}_F(2T) &= \left(e^{-iH_3T_3}e^{-iH_2T_2}e^{-i\frac{\pi-\epsilon}{2}\sum_i X_i}\right)^2 \\ &= e^{-iH_3T_3}e^{-iH_2T_2}e^{i\frac{\epsilon}{2}\sum_i X_i}P_x e^{-iH_3T_3}e^{-iH_2T_2}e^{i\frac{\epsilon}{2}\sum_i X_i}P_x \\ &= \left(e^{-iH_3T_3}e^{-iH_2T_2}e^{i\frac{\epsilon}{2}\sum_i X_i}\right)^2\end{aligned} \tag{29}$$

The remaining terms can be viewed as small perturbations to the original $U_F(2T) = \exp\left[-iH_2T_2\right]^2$. If the perturbation is sufficiently small such that $\tilde{U}_F(2T)$ can achieve MBL, then the system will not thermalise. Since perturbations preserve Ising symmetry P_x, the local unitary V in Section 2.3 will also commute with P_x, hence $\tilde{P}_x = P_x$ [1, p. 40].

2.3.2 Symmetry-Breaking Perturbation

For $g = \frac{\pi}{2}, h_i^x = 0, h_i^z \neq 0$, the Ising symmetry P_x is broken. Because Z_i, X_i anti-commute and Z_i, D_i commute, the Floquet unitary is

$$\begin{aligned}\tilde{U}_F &= \exp\left[-i\sum_j\left(J_iD_i + h_i^zZ_i\right)\right]P_x \\ &= \exp\left[i\sum_j\frac{h_i^z}{2}Z_i\right]\exp\left[-i\sum_j J_iD_i\right]P_x\exp\left[-i\sum_j\frac{h_i^z}{2}Z_i\right] \\ &\equiv VU_FV^\dagger\end{aligned} \tag{30}$$

where we identify $V = \exp\left[i\sum_j \frac{h_i^z}{2} Z_i\right]$, using the fact that $VP_x = P_x V^\dagger$. This allows us to construct the dressed operators as per 2.3. Since $\tilde{U}_F = VUV^\dagger$, the quasienergy spectrum is preserved - eigenstates are cat states with a π gap. Furthermore, the dynamical behaviour at even periods are exactly preserved,

$$\begin{aligned}\tilde{U}_F(2T) &= \exp\left[-i\sum_j (J_i D_i + h_i^z Z_i)\right] P_x \exp\left[-i\sum_j (J_i D_i + h_i^z Z_i)\right] P_x \\ &= \exp\left[-i\sum_j J_i D_i\right] P_x \exp\left[-i\sum_j J_i D_i\right] P_x = U_F(2T)\end{aligned} \tag{31}$$

where the symmetry-breaking perturbation has been "echoed" out by the spin flips P_x. Hence the system cannot thermalise similar to the previous case.

2.4 Observables and distinguishing Signatures

We have shown that the πSG phase of the driven random Ising Model exhibits MBL under perturbations of h_i^z, h_i^x and of flip angle $\pi - \epsilon$. Now we discuss the behaviour of observables and predicted experimental signatures in order to detect this phase, restricted to the case of starting with a generic short-range correlated Z product state $|\alpha\rangle = |\uparrow\downarrow ...\rangle$, only using Pauli operators X, Z, and taking the limits $\lim_{|i-j|\to\infty} \lim_{L\to\infty}$.

2.4.1 Discrete Time Crystal Order

Since πSG is a spin glass phase, it does not exhibit any spatial order and hence cannot display spatio-temporal order (Eq 2). A system displaying DTC order should preserve information about its initial glassy state in addition to period-doubled dynamics. This motivates the following definition:

Definition: A state $|\psi\rangle$ driven by a Floquet unitary U_F of period T displays **Discrete Time Crystal (DTC) Order** if there exist a local observable $O(\vec{x}, t)$ such that $\lim_{|\vec{x}-\vec{x}'|\to\infty} \lim_{V\to\infty} \langle\psi| O(\vec{x}, 0)O(\vec{x}', 0) |\psi\rangle \neq 0$ and

$$\lim_{|\vec{x}-\vec{x}'|\to\infty} \lim_{V\to\infty} \frac{\langle\psi| O(\vec{x}, t)O(\vec{x}', 0) |\psi\rangle}{\langle\psi| O(\vec{x}, 0)O(\vec{x}', 0) |\psi\rangle} \to f(t) \tag{32}$$

converges to a non-vanishing periodic function $f(t)$ with period $T' = nT$ with integer $n > 1$.

Similar to section 1.2, we identify a system as a **Discrete Time Crystal (DTC)** if:

1. all product states $|\alpha\rangle$ display DTC order with the same local observable $O(\vec{x}, t)$ and periodic function $f(t)$,

2. $f(t)$ is not changed when parameters are perturbed such that all symmetries of the drive, except for the period T, are removed.

For example, if $O = X$, this introduces a spin flip that can only be corrected by another spin flip at the same location. However in the limit $\lim_{|i-j|\to\infty} \lim_{L\to\infty}$, the spin flips introduced at locations i, j are much further apart than the support of $X_i(t) = (\tilde{U}_F^\dagger)^n X_i (\tilde{U}_F)^n$ at any finite time nT. Therefore $\langle\alpha| X_i(nT)X_j(0) |\alpha\rangle \to 0$ is not a useful dynamical signature.

2.4.2 Period-Doubled Dynamics

Starting with a product state $|\{z_i\}\rangle = |\uparrow\downarrow ...\rangle$, $\langle\{z_i\}| Z_i(0)Z_j(0) |\{z_i\}\rangle = z_i z_j$ is deterministic. Hence a state $|\{z_i\}\rangle$ will display DTC order if all Z_i autocorrelators display DTTSB oscillations $f(t)$:

$$\frac{\langle\psi| Z_i(nT)Z_j(0) |\psi\rangle}{\langle\psi| Z_i(0)Z_j(0) |\psi\rangle} = \frac{\langle\psi| Z_i(nT) |\psi\rangle}{z_i} = \langle\psi| Z_i(nT)Z_i(0) |\psi\rangle = f(t) \tag{33}$$

Having fixed a starting configuration, measuring the local magnetisation $\langle\{z_i\}|\, Z_i(nT)\, |\{z_i\}\rangle$ is sufficient to determine the DTC correlator and the autocorrelator. This is measured by allowing the experiment to run for n periods, then measuring the gate Z_i (producing a 1 or -1 outcome). Repeating this many times and averaging the result produces $\langle Z_i\rangle_{\{z_i\}}$.

Since $\tilde{\tau}_i$ and Z_i has significant overlap and $\tilde{\tau}_i(nT) = (-1)^n\tilde{\tau}_i$, we expect that $\langle Z_i\rangle$ also exhibits period-doubled dynamics, identified by a sharp peak at π/T in its Discrete Fourier Transform. In practice, the time evolution of $\langle Z_i\rangle$ is bounded by an exponentially decaying envelope due to environmental decoherence. It is possible to use an "echo" procedure (section 3.2.1) to isolate the effects of decoherence.

Crystalline Fraction: The ratio of the DFT intensity at π/T to the total spectral power [30]. A high fraction indicates that the period-doubled dynamics is dominant.

Other methods of analysing the Fourier spectrum include:
- distribution of frequency peaks, regularised by integrating over a small width [28];
- using peak height variance to identify phase transitions [31].

2.4.3 Spin Glass Order Parameter

The most important ingredient for MBL is disorder in the couplings J_i, which produces a spin glass. This phase of matter can be identified in numerical simulation [32] using the **Spin Glass Order Parameter** for a Floquet eigenstate $|\psi\rangle$:

$$\chi^{SG}_{\psi} = \frac{1}{L}\sum_{i,j}\langle\psi|\, Z_iZ_j\, |\psi\rangle^2 \tag{34}$$

In the paramagnetic phase where eigenstates are of the form $|\rightarrow ... \leftarrow\rangle$, the summand is only of $O(1)$ size when $i = j$, causing $\chi^{SG} \sim O(1)$. In the spin glass phase, all L^2 summands are of $O(1)$ size, hence $\chi^{SG} \sim O(L)$ is extensive.

Assuming *Quantum Typicality* [33], we can obtain the measurement of spectrally-averaged quantities with exponentially high accuracy from pure states [34, App. V] produced by a scrambling circuit, averaged over many iterations and disorder realisations.

2.4.4 Level Spacing Statistic

The inter-doublet level-spacing statistic r is defined as:

$$r = \frac{\min_n\{E_{n+2} - E_{n+1}, E_{n+1} - E_n\}}{\max_n\{E_{n+2} - E_{n+1}, E_{n+1} - E_n\}} \tag{35}$$

In MBL, we expect no level repulsion as the quasienergies are independently distributed. This results in a Poisson / exponential distribution for consecutive level spacings [35] (Appendix F). It has mean $\mathbb{E}[r] = 2\ln 2 - 1$ (Appendix F.1).

2.4.5 Initial State Dependence of Lifetime

A key feature of MBL is that **all** eigenstates are localised, and hence any initial state should exhibit similar dynamics as well as decay lifetimes. All of the above discussions were subject to exponentially small errors. However, this means that with exponentially long time, effects of these errors can cause the system to thermalise. If we find states with very different lifetimes of period-doubled dynamics before decay, that indicates that they started at different places along the thermalisation process. This is called "Prethermal Time Crystal" (Fig 6) [36, 37].

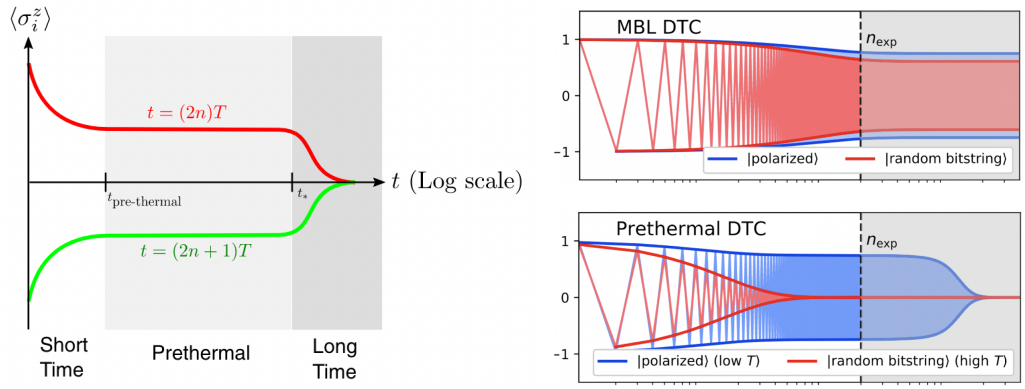

(a) (b)

Figure 6: (a) The order parameter exhibit period-doubled dynamics (red: even times, green: odd times) up to some lifetime t_* before decaying. Figure adapted from [36]. (b) In a truly MBL Discrete Time Crystal, all initial states show period-doubled dynamics up to infinite times. In a Prethermal Time Crystal, a random bit string (corresponding to high temperature) has a significantly shorter lifetime than the fully polarised initial state (low temperature). Figure adapted from [28].

3 Experimental Verification

3.1 First Generation

The theoretical prediction of πSG DTC phase was rapidly followed by the following experiments, each of which simulates a model of Eq 21 with a mix of spatial dimension, interaction range, nature of disorder, and on-site measurement capabilities. They were all able to observe period-doubling robust to certain perturbations, but some lack certain ingredients that are theoretically needed for a genuine MBL DTC phase [28].

3.1.1 Trapped Ions

The experiment in [38] utilises a chain of $N = 10, 12, 14$ trapped ions. Note that their setup uses $J_{ij}X_iX_j$ to orient the spins along the x-direction, and Y_i to flip them. When translated into the orientation used in section 2, we obtain Eq 21, 22. Two initial states were investigated: fully polarised $|00...0\rangle$, and $|0..01..1\rangle$. The single-site magnetisation $\langle Z_i \rangle$ is measured using spin-dependent fluorescence and site-resolved imaging [39, p. 4]. They were able to observe time-crystalline signature in all single-ion magnetisations.

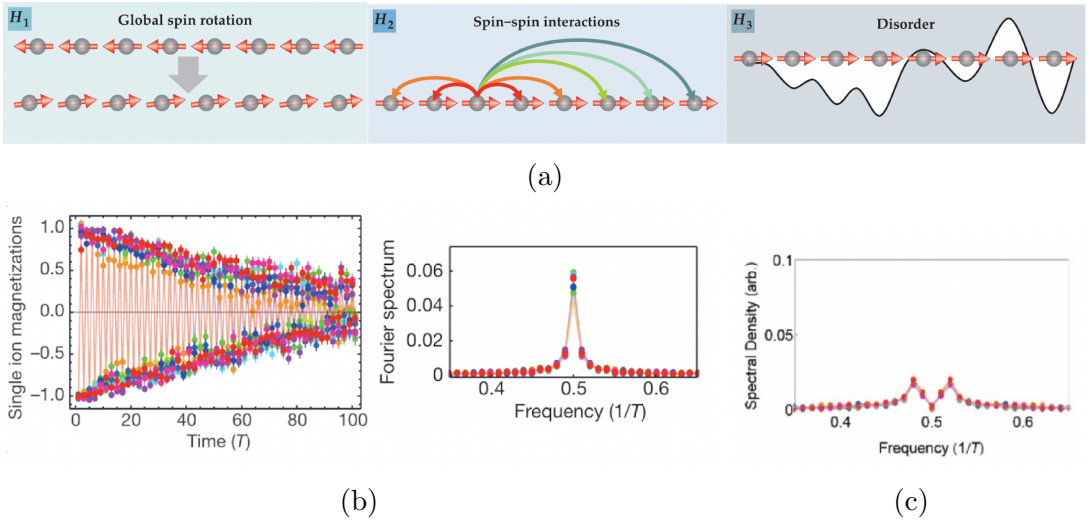

Figure 7: (a) The time evolution is split into 3 steps: a global rotation by $\pi(1-\epsilon)$, spin-spin interactions and on-site disorder. (b) Left panel shows single ion magnetisation $\langle Z_i \rangle$ for each site for 100 periods under interaction and disorder. The oscillations are locked into period-doubled dynamics which can be identified from the Fourier spectrum by a sharp peak at $1/2T$. Each colour represents a trapped ion. (c) With the deterministic interaction only, the Fourier spectrum shows a split peak at $(0.5 \pm \epsilon)/T$. Figures adapted from [40, 38].

However, the system is not in the MBL regime due to the following issues:

- The two-spin couplings are $J_{ij} \propto \frac{J_0}{|i-j|^\alpha}$ with $\alpha = 1.5$, necessarily long-ranged due to the underlying Coulomb interactions between ions. However, as discussed in section 2.2.1, the theoretical requirement of $\alpha > 2d = 2$ is not satisfied here.

- The dominant source of disorder is the **Ising-odd** onsite fields h_i^x rather than the two-spin couplings J_{ij}. Fig 7c shows that with the deterministic interactions J_{ij} only, the Fourier spectrum shows two split peaks at $(0.5 \pm \epsilon)/T$, therefore the system is not synchronised at $1/2T$. As discussed in section 2.3.2, disorder in the on-site fields is insufficient to localise domain walls as Ising-odd perturbations are cancelled out after two periods. Therefore the time-crystalline signature should eventually disappear, but not detectable as it lasts longer than the system's decoherence time of $8ms$ [38].

- Simulations performed by [1] showed strong dependence on initial state for the decay lifetime. States $|0000000000\rangle$ (blue), $|0000011111\rangle$ (red), $|1000110111\rangle$ (black) have lifetime approximately $t = 10^6, 10^5, 10^3 T$ respectively. Simulation for the mean level spacing showed a flow towards the thermal value 0.54, rather than the Poisson value 0.386 (Appendix F) for the entire range of ϵ, as system size increased.

3.1.2 NV Centers

Nitrogen Vacancy (NV) centers are point defects in a diamond crystal, where a pair of carbon atoms are replaced with a nitrogen atom and a lattice vacancy. Each NV center results in a spin-1 system with three levels, two of which can be isolated to form an effective spin 1/2 qubit. Under a sufficiently strong "spin-locking" field, the effective hamiltonian is similar to that of Eq 21 for $\sim 10^6$ lattice sites [30]. Due to the high density of sites, the individual magnetisations cannot be investigated and the only experimental signature is the global magnetisation. This is insufficient to determine MBL as it is a local phenomenon.

The two-spin couplings $J_{ij} \propto \frac{J_0}{|i-j|^3}$ are long-ranged due to the dipole-dipole interactions. J_{ij} is strongly disordered due to factors such as lattice strain, paramagnetic impurities, and random spatial positions of NV centers. Despite this, because of $\alpha = d$ and $d > 1$, it is theoretically not possible to achieve MBL as discussed in section 2.2.1.

Two initial states were investigated, both of which exhibited period-doubled oscillations but only for a short lifetime ($49.2 \pm 3.3\mu s$ and $47.6 \pm 2.4\mu s$). Nevertheless, this experiment is important as it showed that it is possible to replace the spin-flip by cycling through all three levels, thus creating *period-tripled* oscillations of the global magnetisation.

3.1.3 NMR

The experiment performed in [41] uses a 100% occupied crystal lattice, leading to an ordered dipolar system. This lacks many of the conditions for MBL: the dipole-dipole interactions decay with $\alpha = d$, and there is no disorder in the couplings J_{ij}. Nevertheless, period doubling was observed. In [37], it was shown to be the result of a long-lived approximate emergent U(1) symmetry. We will not qualify this as a true DTC as it relies on the breaking of another symmetry, similar to the AC Josephson effect (section 1.3.1).

3.1.4 Programmable Quantum Simulators

The issues above were overcome in a system of 27 ^{13}C nuclear spins in diamond, close to NV centers. Using a subset of 9 spins such that their interactions are disordered and short-ranged $J_{ij} \sim |i-j|^{-2.5}$, this maps approximately onto a 1D system whose interaction falls off sufficiently fast for the possibility of MBL ($\alpha > 2d = 2$). A uniform external magnetic field B is also applied in the z-direction. The Floquet drive is symmetrised as follows:

$$\begin{aligned} U_F &= U_{int} \cdot U_x \cdot U_{int} \\ U_{int} &= \exp[-iH_{int}\tau] \\ H_{int} &= \sum_i (B + h_i) Z_i + \sum_{ij} J_{ij} Z_i Z_j \\ U_x &= \exp\left[-i\frac{g}{2}\sum_i X_i\right] \end{aligned} \tag{36}$$

The strength of interactions are augmented by the interaction drive duration τ. The site-averaged correlation $\bar{\chi} = \frac{1}{L}\sum_{i=1}^{L} \langle Z_i(NT)\rangle \langle Z_i(0)\rangle$ and its Fourier spectrum is analysed in Fig 8.

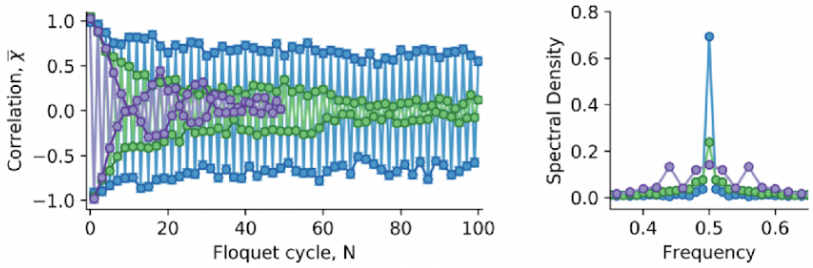

Figure 8: For $g = 0.95\pi$ and initial state $|\uparrow\uparrow\uparrow\uparrow\uparrow\uparrow\uparrow\uparrow\rangle$, increasing the strength of interactions by increasing the driving duration τ (purple $\tau = 0$, green $\tau = 1.55ms$, blue $\tau = 5ms$) is able to stabilise the oscillations and prevent thermalisation. The Fourier spectrum shows a sharp peak at 0.5 for $\tau = 5ms$ (blue), indicated that the system is locked into period-doubled oscillation despite the imperfect spin flip. Figure adapted from [42].

Period doubling for 10^3 cycles (around 10 seconds) was observed, which is roughly at the limit of the environmental decoherence ($1/e$ decay lifetime of 4.7s). $\bar{\chi}$ for 10 randomly chosen initial states showed the same decay envelope and lifetime [42, p. 5]. Based on the aforementioned signatures, system is exhibiting DTC order, although the number of qubits is insufficient to be a truly many-body system.

The key assumption of the dimensionality argument (Appendix E.1) is that the number of interacting spins within a shell of radius $[r, r + dr]$ is proportional to the strength of interaction multiplied by the volume of the shell. In this case, carefully selecting a 1D chain out of a 3D system invalidates this assumption, but makes it more difficult to scale up to larger systems. Even though arbitrary initial product states can be prepared, only spins 2, 5, 6, 8 are directly addressable while the others are weakly coupled to the NV, requiring a spin-echo double resonance protocol [42, 43].

3.2 Second Generation

Since the theory in DTC order only requires Pauli gates, the Hamiltonian is much more naturally realised on qubit circuits in a quantum computer which can provide arbitrary state preparation, individual site addressability, and sufficiently many qubits to exhibit truly many-body behaviour. Three experiments have been conducted on the superconducting transmon qubit architecture [34, 44, 31].

Here we focus on the experiment [34] on Google's Sycamore quantum computer, where a nearest-neighbour coupled chain of $L = 20$ qubits is isolated from a two-dimensional grid. The Floquet unitary is

$$U_F = \exp\left[-\frac{i}{2}\sum_i h_i Z_i\right] \exp\left[-\frac{i}{4}\sum_i J_i Z_i Z_{i+1}\right] \exp\left[-\frac{i\pi}{2} g \sum_i X_i\right] \tag{37}$$

with couplings $J_i \in [-1.5\pi, -0.5\pi], h_i \in [-\pi, \pi]$ sampled randomly. Note that this enforces a ferromagnetic preference (neighbouring spins are aligned). Randomness in J_i creates MBL which persists in imperfect spin flips up to a critical value $g_c \approx 0.84$.

The measurements of magnetisation $\langle Z_i \rangle$ are collated into the autocorrelator $A(nT) = \langle Z(0)Z(nT)\rangle$. Averaging over random bit strings produces $\bar{A}$. The lifetimes of different initial states (polarised $|00..0\rangle$, Neel $|0101...01\rangle$, and random bit strings) were the same in the presence of disorder.

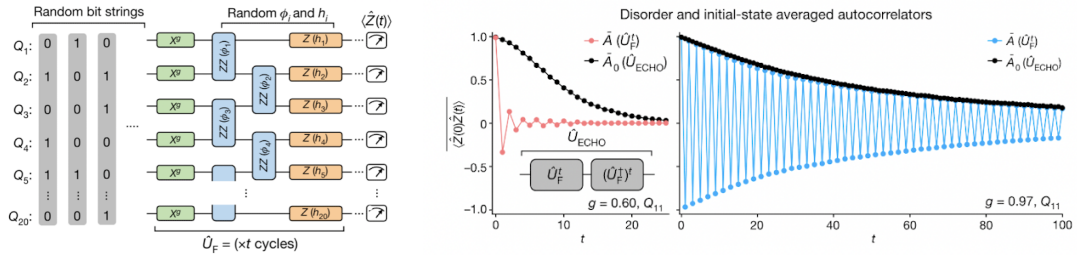

(a) (b)

Figure 9: (a) The circuit schematics for U_F: the action on a random input bit string is split into three steps: a rotation X^g on each qubit, ZZ interactions, and on-site Z disorder. After n cycles, the magnetisation $\langle Z \rangle$ is measured. (b) The disorder and initial-state averaged autocorrelators $\bar{A}$ for $g = 0.60$ (pink) in the thermal regime, and $g = 0.97$ (blue) in the DTC regime. The amplitude of oscillations in DTC regime closely tracks $\bar{A}_0$ (black) obtained by the echo procedure. Adapted from [34].

3.2.1 Echo Dynamics

The present day NISQ devices face limitations on their finite coherence time and gate errors, which represent undesired external and internal interactions. To understand the effects of environmental decoherence, an echo procedure is used: the system is evolved under U_F for n steps, then reversed.

$$U_{ECHO}(2nT) = (U_F^\dagger)^n (U_F)^n \tag{38}$$

The autocorrelator A_0, capturing no dynamics but only the effects of external decoherence and slow internal thermalisation, is then measured. The square root accounts for the fact that U_{ECHO} acts for twice as long as U_F. The

$$A_0(nT) \equiv \sqrt{\langle Z(0)Z(2nT)\rangle} = \sqrt{\langle ZU^{\dagger}_{ECHO}ZU_{ECHO}\rangle} \tag{39}$$

3.2.2 Identifying Phase Transition from Spin Glass Order Parameter

Fig 10 shows the disorder-averaged Spin Glass order parameter χ^{SG}, found by sampling random states under the assumption of quantum typicality. The inset shows that χ^{SG} decreases with number of qubits at $g = 0.78$ and increases with $g = 0.90$. The data indicates a phase transition within the region $0.83 \leq g_c \leq 0.88$.

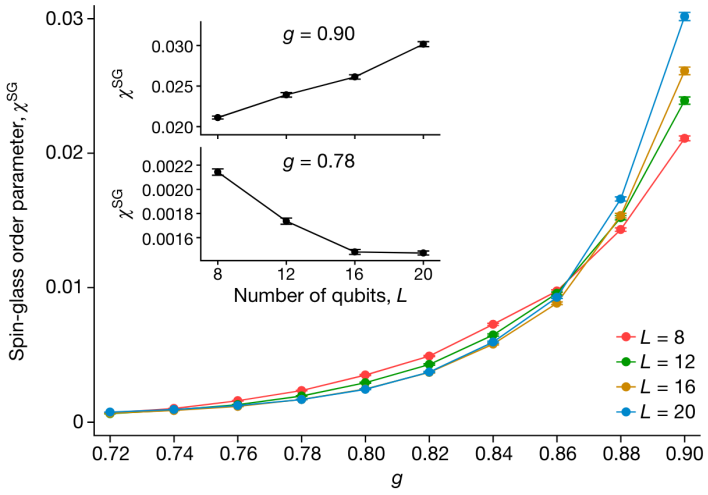

Figure 10: Spin Glass order parameter χ^{SG} increases exponentially as $g \to 1$. This shows that the DTC phase transition is somewhere in-between. Adapted from [34].

3.2.3 Suggestion for Improvements

- Analyse the Fourier transform of the response and the frequency-space peak, such as the Crystalline Fraction f.

- Compare the decay lifetimes of different states, with various values of J_i and distributions to ensure that the effect is only due to disorder and not the magnitude of J_i.

- Confirm that the spin glass order parameter χ^{SG} approaches an extensive value as $g \to 1$.

- Perform simulations to verify the distribution of the level spacing statistic r.

4 Summary

In this essay, we set out to find an example of time translation symmetry breaking. We first examined continuous time translation symmetry for isolated systems and saw that spatio-temporal order (Eq 2) cannot be achieved. In driven Floquet systems, we were able to break the discrete time translation symmetry using Many-Body Localisation (MBL), a phenomenon previously established in isolated systems that prevents thermalisation. We established an Ising model driven by periodic global spin flip. The πSG phase was identified as a candidate for Discrete Time Crystal (DTC), as it has a non-degenerate quasienergy spectrum and long-range correlated eigenstates which satisfy the requirements in Theorem 2 (section 1.4.2). We demonstrated the formation of logical bits and emergent Ising symmetry, key ingredients needed for MBL. Taking into account the spin-glass spatial distribution and periodic temporal behaviour, we defined the Discrete Time Crystal order (Eq 32) needed to detect this phenomenon. Several other experimental signatures were also discussed.

The first generation of experiments based in physical systems had several limitations which meant they were not able to display true MBL, the most important detriment being long-ranged interactions (Appendix E). These were overcome by [42], but the complex procedure needed to isolate a 1D spin chain from a 3D systems severely limits its ability to scale up into a truly many-body regime. The second generation of experiments conducted on quantum computers were much better suited to implementing the theoretical model, with the advantage of arbitrary state preparation and individual site addressability. We concluded that a MBL DTC was truly realised by [34], with minor suggestions raised to verify the results for other diagnostic statistics.

Since their inception in 2012 by Wilczek [45], research into time crystals has yielded fascinating insights into Floquet-enriched many-body phenomena. This has inspired proposals and experiments to probe Floquet-enriched topological order, such as topologically-ordered time crystals [2, 3], dynamical anyon permutation [46], and Floquet error correcting codes [47].

References

[1] V. Khemani, R. Moessner, and S. L. Sondhi, "A brief history of time crystals." http://arxiv.org/abs/1910.10745.

[2] T. B. Wahl and B. Béri, *Local integrals of motion for topologically ordered many-body localized systems*, https://link.aps.org/doi/10.1103/PhysRevResearch.2.033099. Publisher: American Physical Society.

[3] L. Xiang, W. Jiang, Z. Bao, Z. Song, S. Xu, K. Wang, J. Chen, F. Jin, X. Zhu, Z. Zhu, F. Shen, N. Wang, C. Zhang, Y. Wu, Y. Zou, J. Zhong, Z. Cui, A. Zhang, Z. Tan, T. Li, Y. Gao, J. Deng, X. Zhang, H. Dong, P. Zhang, S. Jiang, W. Li, Z. Lu, Z.-Z. Sun, H. Li, Z. Wang, C. Song, Q. Guo, F. Liu, Z.-X. Gong, A. V. Gorshkov, N. Y. Yao, T. Iadecola, F. Machado, H. Wang, and D.-L. Deng, "Long-lived topological time-crystalline order on a quantum processor." http://arxiv.org/abs/2401.04333.

[4] H. Watanabe and M. Oshikawa, *Absence of quantum time crystals*, https://link.aps.org/doi/10.1103/PhysRevLett.114.251603. Publisher: American Physical Society.

[5] B. Béri, *Topological quantum matter - lecture notes,*. University of Cambridge.

[6] Z.-J. Zhang, J. Sun, X. Yuan, and M.-H. Yung, *Low-depth hamiltonian simulation by an adaptive product formula*, https://link.aps.org/doi/10.1103/PhysRevLett.130.040601. Publisher: American Physical Society.

[7] D. W. Berry, A. M. Childs, R. Cleve, R. Kothari, and R. D. Somma, *Simulating hamiltonian dynamics with a truncated taylor series*, https://link.aps.org/doi/10.1103/PhysRevLett.114.090502.

[8] J. Bardeen, L. N. Cooper, and J. R. Schrieffer, *Theory of superconductivity*, https://link.aps.org/doi/10.1103/PhysRev.108.1175. Publisher: American Physical Society.

[9] M. Greiter, *Is electromagnetic gauge invariance spontaneously violated in superconductors?*, https://www.sciencedirect.com/science/article/pii/S0003491605000515.

[10] M. P. Zaletel, M. Lukin, C. Monroe, C. Nayak, F. Wilczek, and N. Y. Yao, *Colloquium: Quantum and classical discrete time crystals*, https://link.aps.org/doi/10.1103/RevModPhys.95.031001. Publisher: American Physical Society.

[11] D. V. Else, C. Monroe, C. Nayak, and N. Y. Yao, *Discrete time crystals*, https://www.annualreviews.org/content/journals/10.1146/annurev-conmatphys-031119-050658. Publisher: Annual Reviews.

[12] P. Kongkhambut, J. Skulte, L. Mathey, J. G. Cosme, A. Hemmerich, and H. Keßler, *Observation of a continuous time crystal*, https://www.science.org/doi/10.1126/science.abo3382. Publisher: American Association for the Advancement of Science.

[13] V. Khemani, A. Lazarides, R. Moessner, and S. Sondhi, *Phase structure of driven quantum systems*, https://link.aps.org/doi/10.1103/PhysRevLett.116.250401. Publisher: American Physical Society.

[14] K. Viebahn, "Introduction to floquet theory.".

[15] D. V. Else, B. Bauer, and C. Nayak, *Floquet time crystals*, https://link.aps.org/doi/10.1103/PhysRevLett.117.090402. Publisher: American Physical Society.

[16] J. M. Deutsch, *Quantum statistical mechanics in a closed system*, https://link.aps.org/doi/10.1103/PhysRevA.43.2046. Publisher: American Physical Society.

[17] M. Srednicki, *Chaos and quantum thermalization*, https://link.aps.org/doi/10.1103/PhysRevE.50.888. Publisher: American Physical Society.

[18] M. Rigol, V. Dunjko, and M. Olshanii, *Thermalization and its mechanism for generic isolated quantum systems*, https://www.nature.com/articles/nature06838. Publisher: Nature Publishing Group.

[19] J. Z. Imbrie, V. Ros, and A. Scardicchio, *Local integrals of motion in many-body localized systems*, https://onlinelibrary.wiley.com/doi/abs/10.1002/andp.201600278.

[20] D. A. Huse, R. Nandkishore, and V. Oganesyan, *Phenomenology of fully many-body-localized systems*, https://link.aps.org/doi/10.1103/PhysRevB.90.174202. Publisher: American Physical Society.

[21] M. Serbyn, Z. Papić, and D. A. Abanin, *Universal slow growth of entanglement in interacting strongly disordered systems*, https://link.aps.org/doi/10.1103/PhysRevLett.110.260601. Publisher: American Physical Society.

[22] E. H. Lieb and D. W. Robinson, *The finite group velocity of quantum spin systems*, https://doi.org/10.1007/BF01645779.

[23] J. Z. Imbrie, *On many-body localization for quantum spin chains*, https://doi.org/10.1007/s10955-016-1508-x.

[24] V. Subrahmanyam, *Domain wall dynamics of the ising chain in a transverse field*, https://link.aps.org/doi/10.1103/PhysRevB.68.212407. Publisher: American Physical Society.

[25] W. De Roeck and F. Huveneers, *Stability and instability towards delocalization in many-body localization systems*, https://link.aps.org/doi/10.1103/PhysRevB.95.155129. Publisher: American Physical Society.

[26] S. Gopalakrishnan and D. A. Huse, *Instability of many-body localized systems as a phase transition in a nonstandard thermodynamic limit*, https://link.aps.org/doi/10.1103/PhysRevB.99.134305. Publisher: American Physical Society.

[27] C. W. von Keyserlingk and S. L. Sondhi, *Phase structure of one-dimensional interacting floquet systems. i. abelian symmetry-protected topological phases*, https://link.aps.org/doi/10.1103/PhysRevB.93.245145. Publisher: American Physical Society.

[28] M. Ippoliti, K. Kechedzhi, R. Moessner, S. Sondhi, and V. Khemani, *Many-body physics in the NISQ era: Quantum programming a discrete time crystal*, https://link.aps.org/doi/10.1103/PRXQuantum.2.030346. Publisher: American Physical Society.

[29] C. W. von Keyserlingk, V. Khemani, and S. L. Sondhi, *Absolute stability and spatiotemporal long-range order in floquet systems*, https://link.aps.org/doi/10.1103/PhysRevB.94.085112. Publisher: American Physical Society.

[30] S. Choi, J. Choi, R. Landig, G. Kucsko, H. Zhou, J. Isoya, F. Jelezko, S. Onoda, H. Sumiya, V. Khemani, C. von Keyserlingk, N. Y. Yao, E. Demler, and M. D. Lukin, *Observation of discrete time-crystalline order in a disordered dipolar many-body system*, https://www.nature.com/articles/nature21426. Number: 7644 Publisher: Nature Publishing Group.

[31] H. Xu, J. Zhang, J. Han, Z. Li, G. Xue, W. Liu, Y. Jin, and H. Yu, "Realizing discrete time crystal in an one-dimensional superconducting qubit chain." http://arxiv.org/abs/2108.00942.

[32] J. A. Kjäll, J. H. Bardarson, and F. Pollmann, *Many-body localization in a disordered quantum ising chain*, https://link.aps.org/doi/10.1103/PhysRevLett.113.107204. Publisher: American Physical Society.

[33] C. Bartsch and J. Gemmer, *Dynamical typicality of quantum expectation values*, https://link.aps.org/doi/10.1103/PhysRevLett.102.110403. Publisher: American Physical Society.

[34] X. Mi, M. Ippoliti, C. Quintana, A. Greene, Z. Chen, J. Gross, F. Arute, K. Arya, J. Atalaya, R. Babbush, J. C. Bardin, J. Basso, A. Bengtsson, A. Bilmes, A. Bourassa, L. Brill, M. Broughton, B. B. Buckley, D. A. Buell, B. Burkett, N. Bushnell, B. Chiaro, R. Collins, W. Courtney, D. Debroy, S. Demura, A. R. Derk, A. Dunsworth, D. Eppens, C. Erickson, E. Farhi, A. G. Fowler, B. Foxen, C. Gidney, M. Giustina, M. P. Harrigan, S. D. Harrington, J. Hilton, A. Ho, S. Hong, T. Huang, A. Huff, W. J. Huggins, L. B. Ioffe, S. V. Isakov, J. Iveland,

E. Jeffrey, Z. Jiang, C. Jones, D. Kafri, T. Khattar, S. Kim, A. Kitaev, P. V. Klimov, A. N. Korotkov, F. Kostritsa, D. Landhuis, P. Laptev, J. Lee, K. Lee, A. Locharla, E. Lucero, O. Martin, J. R. McClean, T. McCourt, M. McEwen, K. C. Miao, M. Mohseni, S. Montazeri, W. Mruczkiewicz, O. Naaman, M. Neeley, C. Neill, M. Newman, M. Y. Niu, T. E. O'Brien, A. Opremcak, E. Ostby, B. Pato, A. Petukhov, N. C. Rubin, D. Sank, K. J. Satzinger, V. Shvarts, Y. Su, D. Strain, M. Szalay, M. D. Trevithick, B. Villalonga, T. White, Z. J. Yao, P. Yeh, J. Yoo, A. Zalcman, H. Neven, S. Boixo, V. Smelyanskiy, A. Megrant, J. Kelly, Y. Chen, S. L. Sondhi, R. Moessner, K. Kechedzhi, V. Khemani, and P. Roushan, *Time-crystalline eigenstate order on a quantum processor*, https://www.nature.com/articles/s41586-021-04257-w. Publisher: Nature Publishing Group.

[35] D. A. Huse, R. Nandkishore, V. Oganesyan, A. Pal, and S. L. Sondhi, *Localization-protected quantum order*, https://link.aps.org/doi/10.1103/PhysRevB.88.014206.

[36] D. V. Else, B. Bauer, and C. Nayak, *Prethermal phases of matter protected by time-translation symmetry*, https://link.aps.org/doi/10.1103/PhysRevX.7.011026. Publisher: American Physical Society.

[37] D. J. Luitz, R. Moessner, S. Sondhi, and V. Khemani, *Prethermalization without temperature*, https://link.aps.org/doi/10.1103/PhysRevX.10.021046. Publisher: American Physical Society.

[38] J. Zhang, P. W. Hess, A. Kyprianidis, P. Becker, A. Lee, J. Smith, G. Pagano, I.-D. Potirniche, A. C. Potter, A. Vishwanath, N. Y. Yao, and C. Monroe, *Observation of a discrete time crystal*, https://www.nature.com/articles/nature21413. Number: 7644 Publisher: Nature Publishing Group.

[39] C. Monroe, W. C. Campbell, L.-M. Duan, Z.-X. Gong, A. V. Gorshkov, P. Hess, R. Islam, K. Kim, N. Linke, G. Pagano, P. Richerme, C. Senko, and N. Y. Yao, *Programmable quantum simulations of spin systems with trapped ions*, 1912.07845 [cond-mat, physics:quant-ph], http://arxiv.org/abs/1912.07845.

[40] N. Y. Yao and C. Nayak, *Time crystals in periodically driven systems*, https://doi.org/10.1063/PT.3.4020.

[41] J. Rovny, R. L. Blum, and S. E. Barrett, *Observation of discrete-time-crystal signatures in an ordered dipolar many-body system*, 1802.00126 [cond-mat, physics:quant-ph], http://arxiv.org/abs/1802.00126.

[42] J. Randall, C. E. Bradley, F. V. van der Gronden, A. Galicia, M. H. Abobeih, M. Markham, D. J. Twitchen, F. Machado, N. Y. Yao, and T. H. Taminiau, *Observation of a many-body-localized discrete time crystal with a programmable spin-based quantum simulator*, 2107.00736 [cond-mat, physics:quant-ph], http://arxiv.org/abs/2107.00736.

[43] C. Bradley, J. Randall, M. Abobeih, R. Berrevoets, M. Degen, M. Bakker, M. Markham, D. Twitchen, and T. Taminiau, *A ten-qubit solid-state spin register*

with quantum memory up to one minute, https://link.aps.org/doi/10.1103/PhysRevX.9.031045. Publisher: American Physical Society.

[44] P. Frey and S. Rachel, *Realization of a discrete time crystal on 57 qubits of a quantum computer*, https://www.science.org/doi/10.1126/sciadv.abm7652. Publisher: American Association for the Advancement of Science.

[45] F. Wilczek, *Quantum time crystals*, https://link.aps.org/doi/10.1103/PhysRevLett.109.160401. Publisher: American Physical Society.

[46] A. C. Potter and T. Morimoto, *Dynamically enriched topological orders in driven two-dimensional systems*, https://link.aps.org/doi/10.1103/PhysRevB.95.155126. Publisher: American Physical Society.

[47] A. Fahimniya, H. Dehghani, K. Bharti, S. Mathew, A. J. Kollár, A. V. Gorshkov, and M. J. Gullans, "Fault-tolerant hyperbolic floquet quantum error correcting codes." http://arxiv.org/abs/2309.10033.

[48] N. Yao, C. Laumann, S. Gopalakrishnan, M. Knap, M. Müller, E. Demler, and M. Lukin, *Many-body localization in dipolar systems*, https://link.aps.org/doi/10.1103/PhysRevLett.113.243002. Publisher: American Physical Society.

[49] R. M. Nandkishore and S. Sondhi, *Many-body localization with long-range interactions*, https://link.aps.org/doi/10.1103/PhysRevX.7.041021. Publisher: American Physical Society.

[50] F. Machado, G. D. Kahanamoku-Meyer, D. V. Else, C. Nayak, and N. Y. Yao, *Exponentially slow heating in short and long-range interacting floquet systems*, https://link.aps.org/doi/10.1103/PhysRevResearch.1.033202. Publisher: American Physical Society.

[51] G. Kucsko, S. Choi, J. Choi, P. Maurer, H. Zhou, R. Landig, H. Sumiya, S. Onoda, J. Isoya, F. Jelezko, E. Demler, N. Yao, and M. Lukin, *Critical thermalization of a disordered dipolar spin system in diamond*, https://link.aps.org/doi/10.1103/PhysRevLett.121.023601. Publisher: American Physical Society.

[52] Y. Y. Atas, E. Bogomolny, O. Giraud, and G. Roux, *Distribution of the ratio of consecutive level spacings in random matrix ensembles*, https://link.aps.org/doi/10.1103/PhysRevLett.110.084101. Publisher: American Physical Society.

[53] L. F. Cugliandolo, "Advanced statistical physics: Random matrices." https://www.lpthe.jussieu.fr/%7Eleticia/TEACHING/Master2017/random-matrices.pdf.

[54] O. Giraud, N. Mace, E. Vernier, and F. Alet, *Probing symmetries of quantum many-body systems through gap ratio statistics*, https://link.aps.org/doi/10.1103/PhysRevX.12.011006. Publisher: American Physical Society.

[55] D. S. Fisher, *Critical behavior of random transverse-field ising spin chains*, https://link.aps.org/doi/10.1103/PhysRevB.51.6411. Publisher: American Physical Society.

Appendix A Proof of Theorem 1

Remarks:

- The key assumption is that the total weight of the operators A, H are of order V. Since they are sums of local operators, their commutator only involves terms which are at approximately the same location. Hence $[H, A]$ is of order V and also a sum of local observables. $[A, [H, A]]$ is also of order V by the same logic. The proof is reproduced in Appendix A.

- Theorem 1 applies to any eigenstate, not just the ground state. However a flaw has been found by (Appendix A [1]) in the proof for a Gibbs ensemble of states at temperature $T > 0$.

Proof:
In the Heisenberg picture, we have

$$\begin{aligned} \langle 0| A(t)B(0) |0\rangle &= \langle 0| e^{iHt}A(0)e^{-iHt}B(0) |0\rangle \\ &= \langle 0| A(0)e^{-i(H-E_0)t}B(0) |0\rangle \end{aligned} \tag{40}$$

Using some algebraic manipulation, we have

$$\begin{aligned} &|\langle 0| A(0)\ e^{-i(H-E_0)t}B(0) |0\rangle - \langle 0| A(0)B(0) |0\rangle| \\ &\quad = \left| \int_0^t ds\ \frac{d}{ds} \langle 0| A(0)e^{-i(H-E_0)s}B(0) |0\rangle \right| \\ &\quad \leq \left| \int_0^t ds\ \langle 0| A(0)(H-E_0)e^{-i(H-E_0)s}B(0) |0\rangle \right| \\ &\quad \leq \int_0^t ds\ \left| \langle 0| A(0)(H-E_0)e^{-i(H-E_0)s}B(0) |0\rangle \right| \\ &\quad = \int_0^t ds\ \left| \langle 0| A(0)(H-E_0)^{\frac{1}{2}}e^{-i(H-E_0)s}(H-E_0)^{\frac{1}{2}}B(0) |0\rangle \right| \end{aligned} \tag{41}$$

The Cauchy-Schwarz Inequality is:

$$\langle\psi|\psi\rangle \langle\phi|\phi\rangle \geq |\langle\psi|\phi\rangle|^2 \tag{42}$$

By identifying $|\psi\rangle = (H-E_0)^{\frac{1}{2}}A(0) |0\rangle$, $|\phi\rangle = e^{-i(H-E_0)s}(H-E_0)^{\frac{1}{2}}B(0) |0\rangle$, where we used the fact that all the operators here are hermitian: $A^\dagger = A, H^\dagger = H$, we have

$$\begin{aligned} &\left| \langle 0| A(0)(H-E_0)^{\frac{1}{2}}e^{-i(H-E_0)s}(H-E_0)^{\frac{1}{2}}B(0) |0\rangle \right| \\ &\leq \sqrt{\langle 0| A(0)(H-E_0)A(0) |0\rangle \langle 0| B(0)(H-E_0)B(0) |0\rangle} \end{aligned} \tag{43}$$

By observing that $[A(0), [H, A(0)]] = 2A(0)HA(0) - HA(0)^2 - A(0)^2H$, and that $H |0\rangle = E_0 |0\rangle$, we have

$$\langle 0| A(0)(H-E_0)A(0) |0\rangle = \frac{1}{2} \langle 0| [A(0), [H, A(0)]] |0\rangle \tag{44}$$

By the argument in the remarks above, Eq 44 is of order V. Hence Eq 43 is of order V, thus there exist a constant C (which depends on the details of $A, B, H, |0\rangle$, but not of volume or time). Hence,

$$\begin{aligned} &\left|\langle 0|\, A(0)\; e^{-i(H-E_0)t} B(0)\,|0\rangle - \langle 0|\, A(0)B(0)\,|0\rangle\right| \\ &\qquad \leq \int_0^t ds\; CV \\ &\qquad = CVt \end{aligned} \tag{45}$$

which then proves Eq 8 and theorem 1 as desired.

Appendix B Thermalisation

Definition: A system initially with density matrix $\rho(0)$ with time-independent hamiltonian H has **inverse temperature** $\beta = \frac{1}{T}$ defined by the solution to:

$$E_{\text{initial}} = Tr[H\rho(0)] \equiv \frac{1}{Z} Tr[He^{-\beta H}] = \langle E \rangle \tag{46}$$

Definition: A system **thermalises** if for all local observables O,

$$\lim_{t\to\infty} \lim_{V\to\infty} Tr[O\rho(t)] = \lim_{V\to\infty} Tr[O\rho_{eq}(\beta, ...)] \tag{47}$$

where ρ_{eq} is the density matrix of the equilibrium ensemble, such as the canonical ensemble $\rho_{eq} = \frac{1}{Z} e^{-\beta H}$, and parameters such as β are defined as above.

Proposed by Deutsch [16] and Srednicki [17], the **Eigenstate Thermalisation Hypothesis (ETH)** states: local observables O evaluated in energy eigenstates $|\alpha\rangle$ vary smoothly as a function of energy density E_α (and other conserved densities), so that eigenstates nearby in energy have identical local properties (up to variations exponentially small in V) [1, p. 12]. Further, eigenstate expectation values agree with expected thermodynamic ensemble averages at the temperature associated with the energy density of the eigenstate $|\psi\rangle$ [18].

$$\langle\psi| O |\psi\rangle = \langle O \rangle_{\text{microcanonical ensemble at } \beta} \tag{48}$$

Under ETH, the expectation value of O for any state $|\alpha\rangle = \sum_a A_a |\psi_a\rangle$ (expanded in terms of eigenstates) approaches this constant value. Not only is the system unable to display DTTSB, one will not be able to distinguish between different initial states at large times, representing a thermal phase of matter.

$$\begin{aligned}
\langle\alpha| O(nT) |\alpha\rangle &= \sum_a \sum_b A_a^* A_b \langle\psi_a| (U_F^\dagger)^n O(0) (U_F)^n |\psi_b\rangle \\
&= \sum_a \sum_b A_a^* A_b e^{-i(\epsilon_b - \epsilon_a)nT} \langle\psi_a| O(0) |\psi_b\rangle \\
&= \sum_a |A_a|^2 \langle\psi_a| O(0) |\psi_a\rangle + \sum_{a\neq b} A_a^* A_b e^{-i(\epsilon_b - \epsilon_a)nT} \langle\psi_a| O_i(0) |\psi_b\rangle \\
&\xrightarrow{ETH, n\to\infty} \sum_a |A_a|^2 \langle O \rangle_{ETH} = \langle O \rangle_{ETH}
\end{aligned} \tag{49}$$

The terms with $a = b$ do not change in time. Under ETH, this can be replaced by the thermodynamic expectation value. On the other hand, the terms with $a \neq b$ represent a sum of (generally non-zero and incommensurate) exponential terms $e^{-i\Delta\epsilon\ nT}$, which will decay as n increases, known as *dephasing*. Note that with finitely many energy levels, the amplitude will "revive" at some large finite time, therefore the large system limit $\lim_{L\to\infty}$ is necessary to ensure dephasing $\sum e^{-i\Delta\epsilon\ nT} \to 0$ [1, pp. 11,26].

Appendix C Existence of Logical Operators

Theorem: There exist N operators I_i, $i = 0, ..., N-1$, such that $I_i^2 = 1, [I_i, I_j] = [H, I_i] = 0$, such that the eigenstates $|0\rangle, ... |2^N - 1\rangle$ of H can be labelled by the eigenvalues $|\{I_i\}\rangle$.

Proof: Assume that in the energy eigenstate basis, the Hamiltonian is represented by a diagonal matrix of *distinct* energy eigenvalues $\text{diag}(E_1, E_2, ...)$. Then if any operator A satisfies $[H, A] = 0$, then it must be diagonal itself. This is because

$$\begin{aligned} [H, A]_{ij} = 0 &\iff \sum_k H_{ik} A_{kj} = \sum_k A_{ik} H_{kj} \\ &\iff E_i A_{ij} = A_{ij} E_j \end{aligned} \tag{50}$$

Hence $A_{ij} = 0$ for $i \neq j$.

Now consider a bijection matching each energy eigenstate $|i\rangle$ with a binary string $B(i)$ of length N corresponding to i. For example, $|0\rangle \equiv 0...00, |1\rangle \equiv 0...01$. We then construct the operator I_k such that the eigenvalue of $|i\rangle$ is $(-1)^{B(i)_k}$, where $B(i)_k$ is the k^{th} digit of the binary string. Since the matrix representation of I_k is diagonal in the energy eigenstate basis, they commute with each other and with the hamiltonian H.

Example:

Binary Encoded Eigenstates	I_0	I_1
$\|00\rangle = \|\uparrow\uparrow\rangle$ $\|01\rangle = \|\uparrow\downarrow\rangle$ $\|10\rangle = \|\downarrow\uparrow\rangle$ $\|11\rangle = \|\downarrow\downarrow\rangle$	Z_0	Z_1
$\|00\rangle = \frac{1}{\sqrt{2}}(\|\uparrow\uparrow\rangle + \|\downarrow\downarrow\rangle)$ $\|01\rangle = \frac{1}{\sqrt{2}}(\|\uparrow\uparrow\rangle - \|\downarrow\downarrow\rangle)$ $\|10\rangle = \frac{1}{\sqrt{2}}(\|\uparrow\downarrow\rangle + \|\downarrow\uparrow\rangle)$ $\|11\rangle = \frac{1}{\sqrt{2}}(\|\uparrow\downarrow\rangle - \|\downarrow\uparrow\rangle)$	$Z_0 Z_1$	$X_0 X_1$
$\|00\rangle = \frac{\sqrt{3}}{2}\|\uparrow\uparrow\rangle + \frac{1}{2}\|\downarrow\downarrow\rangle$ $\|01\rangle = \frac{\sqrt{3}}{2}\|\uparrow\uparrow\rangle - \frac{1}{2}\|\downarrow\downarrow\rangle$ $\|10\rangle = \frac{\sqrt{3}}{2}\|\uparrow\downarrow\rangle + \frac{1}{2}\|\downarrow\uparrow\rangle$ $\|11\rangle = \frac{\sqrt{3}}{2}\|\uparrow\downarrow\rangle - \frac{1}{2}\|\downarrow\uparrow\rangle$	$Z_0 Z_1$	$\frac{2 - Z_0}{\sqrt{3}} X_0 X_1$

From the above examples, we can see that these operators can be complex and non-local. There are also $(2^N)!$ ways to match a state to a binary string, and we can even include complex phases within the eigenvalues.

Appendix D Domain Wall Propagation

In the interaction picture with main hamiltonian $H_z = -\sum_i JZ_iZ_{i+1}$ and interacting part $H_x = -\sum_i hX_i$. Using the identities $X_i^2 = Z_i^2 = 1, [Z_i, X_i] = 2iY_i, [Z_i, Y_i] = -2iX_i$, we begin with the usual proof for the *Hadamard formula*.

$$\begin{aligned} f(s) &= e^{sA}Be^{-sA} \\ \frac{df}{ds} &= Ae^{sA}Be^{-sA} - e^{sA}Be^{-sA}A = [A, f(s)] \\ \Rightarrow f(s) &= B + s[A,B] + \frac{s^2}{2!}[A,[A,B]] + \frac{s^3}{3!}[A,[A,[A,B]]] + ... \end{aligned} \tag{51}$$

Then we have

$$\int_0^t dt\ f(s) = Bt + \frac{t^2}{2!}[A,B] + \frac{t^3}{3!}[A,[A,B]] + \frac{t^4}{4!}[A,[A,[A,B]]] + ... \tag{52}$$

and

$$\left[\sum_j Z_jZ_{j+1}, X_i\right] = [Z_{i-1}Z_i, X_i] + [Z_iZ_{i+1}, X_i] = 2i(Z_{i-1} + Z_{i+1})Y_i \tag{53}$$

$$\left[\sum_j Z_jZ_{j+1}, Y_i\right] = [Z_{i-1}Z_i, Y_i] + [Z_iZ_{i+1}, Y_i] = -2i(Z_{i-1} + Z_{i+1})X_i \tag{54}$$

Combining the above, we have:

$$\begin{aligned} X_i(s) = e^{is\sum_j JZ_jZ_{j+1}}X_ie^{-is\sum_j JZ_jZ_{j+1}} = X_i &+ (isJ)2i(Z_{i-1} + Z_{i+1})Y_i \\ &+ \frac{(isJ)^2}{2!}(2i(Z_{i-1} + Z_{i+1}))(-2i(Z_{i-1} + Z_{i+1})X_i) \\ &+ \frac{(isJ)^3}{3!}(2i(Z_{i-1} + Z_{i+1}))(-2i(Z_{i-1} + Z_{i+1})) \\ &(2i(Z_{i-1} + Z_{i+1})Y_i) + ... \end{aligned} \tag{55}$$

$$\begin{aligned} X_i(s) = X_i &- (2sJ)(Z_{i-1} + Z_{i+1})Y_i \\ &- \frac{(2sJ)^2}{2!}(Z_{i-1} + Z_{i+1})^2X_i \\ &+ \frac{(2sJ)^3}{3!}(Z_{i-1} + Z_{i+1})^3Y_i + ... \end{aligned} \tag{56}$$

$$\begin{aligned} X_i(s) =& X_i\left[1 - \frac{(2sJ)^2}{2!}(Z_{i-1} + Z_{i+1})^2 + \frac{(2sJ)^4}{4!}(Z_{i-1} + Z_{i+1})^4 + ...\right] \\ &- Y_i\left[(2sJ)(Z_{i-1} + Z_{i+1}) - \frac{(2sJ)^3}{3!}(Z_{i-1} + Z_{i+1})^3 + ...\right] \end{aligned} \tag{57}$$

Now let $a_i = (Z_{i-1} + Z_{i+1})$. Then observe $a_i^4 = 4a_i^2, a_i^6 = 4a_i^4 = 16a_i^2$, and $a_i^3 = 4a_i$ etc.

$$
\begin{aligned}
X_i(s) &= X_i\left[1-\frac{1}{4}a_i^2\left(\frac{(4sJ)^2}{2!}-\frac{(4sJ)^4}{4!}+...\right)\right]-Y_ia_i\frac{1}{2}\left[(4sJ)-\frac{(4sJ)^3}{3!}+...\right] \\
&= X_i\left[1-\frac{1}{4}a_i^2\left(1-\cos(4sJ)\right)\right]-Y_ia_i\frac{1}{2}\sin(4sJ)
\end{aligned}
\tag{58}
$$

$$
\begin{aligned}
\int_0^t ds\ X_i(s) &= tX_i\left(1-\frac{1}{4}a_i^2\right)+X_i\frac{a_i^2}{4}\frac{\sin(4Jt)}{4J}-Y_i\frac{a_i}{2}\frac{1-\cos 4sJ}{4J} \\
&= t\left[X_i\left(1-\frac{a_i^2}{4}+\frac{a_i^2}{4}\frac{\sin(4Jt)}{4Jt}\right)-Y_i\frac{a_i}{2}\frac{1-\cos 4Jt}{4Jt}\right]
\end{aligned}
\tag{59}
$$

Hence the unitary time-evolution operator in the interaction picture is:

$$
U(t)=\exp(-i\int_0^t ds\ H_x(s))=\prod_i\exp\left(-i\int_0^t ds\ hX_i(s)\right) \tag{60}
$$

At time $t=\frac{2\pi}{4J}$, we find an effective time-independent hamiltonian H_1,

$$
\begin{aligned}
U\left(t=\frac{2\pi}{4J}\right) &= \exp(-itH_1) \\
H_1 &= \sum_i hX_i\left[1-\frac{1}{4}(Z_{i-1}+Z_{i+1})^2\right] \\
&= \sum_i\frac{hX_i}{2}\left(1-Z_{i-1}Z_{i+1}\right)
\end{aligned}
\tag{61}
$$

For n periods of unitary evolution,

$$
\begin{aligned}
U\left(t=\frac{2n\pi}{4J}\right) &= \exp\left[-i\frac{n\pi h}{4J}\sum_i X_i\left(1-Z_{i-1}Z_{i+1}\right)\right] \\
&= \prod_i\left[\cos\left(\frac{n\pi h}{4J}\right)-i\sin\left(\frac{n\pi h}{4J}\right)X_i\left(1-Z_{i-1}Z_{i+1}\right)\right]
\end{aligned}
\tag{62}
$$

Appendix E Dimensionality and Long-ranged Interactions

E.1 Dimension

Due to the randomly selected J_{ij} values, in the system size limit $V \to \infty$, an "ergodic grain" (Section III C [25]) is likely to exist - a region with anomalously weak disorder, where MBL does not occur. Instead, through exponentially decaying interaction with surrounding l-bits I_i, this acts as a thermal bath.

For an ergodic grain of radius l_b, it is connected to N_l more l-bits:

$$N_l = C_d \left[(l_b + l)^d - l_b^d\right] \tag{63}$$

When these I_i have been thermalised, the bath density of states increases by a factor 2^{N_l}. Hence if $d = 1$, this is exponential $\sim 2^l$. For $d > 1$, this is super-exponential $\sim 2^{l^d}$ and cannot be overcome by exponentially decreasing couplings.

E.2 Power-Law Interaction

For a power-law $J \sim r^{-\alpha}$, [26] discussed the following possibilities. (See also [48, 49, 50])

E.2.1 $\alpha < d$

In a sphere of radius R, the number of spin-spin resonances expected is $R^d \cdot JR^{-\alpha} = JR^{d-\alpha}$. When $\alpha < d$, this diverges in the large system limit, hence such resonances will occur and entangle spins that are far away.

E.2.2 $\alpha = d$

It is shown that this leads to a power-law decay in time [51], for example in dipole-dipole interaction in 3 dimensions. For a particular spin, we assume the probability of finding another spin that is resonant with it within a shell of radius $[r, r + dr]$ is directly proportional to the interaction strength and and shell volume.

Thus the probability of not finding any resonant spins in a region of radius $[r, R]$ is:

$$P = \prod_r^R \left(1 - 4\pi n r^2 \frac{J}{r^3} dr\right) \tag{64}$$

where n is the density of spins that are oppositely polarised to the central spin. More precisely, by dividing the radius into N sections,

$$\begin{aligned} P &= \lim_{N\to\infty} \prod_{i=1}^{N} \left(1 - \frac{k\frac{i}{N}(R-r)}{r + \frac{i}{N}(R-r)}\right) \\ \log P &= \lim_{N\to\infty} \sum_{i=1}^{N} \log\left(1 - \frac{k(R-r)}{Nr + (R-r)}\right) \\ &= \lim_{N\to\infty} \sum_{i=1}^{N} \log\left(1 - \frac{k(\lambda-1)}{N + i(\lambda-1)}\right) \end{aligned} \tag{65}$$

where $\lambda = \frac{R}{r}$ and $k = 4\pi nJ$. Observe that in the series expansion of the summand, terms higher than first order are $\sim O(N^{-2})$. The sum contributes $O(N)$, hence these terms disappear in the limit $N \to \infty$.

$$\begin{aligned}
\log P &= \lim_{N\to\infty} \sum_{i=1}^{N} -\frac{k(\lambda-1)}{N + i(\lambda-1)} \\
&= \lim_{N\to\infty} -\sum_{i=1}^{N} \frac{1}{N} \frac{k(\lambda-1)}{1 + \frac{i}{N}(\lambda-1)} \\
&= -\int_0^1 \frac{k(\lambda-1)}{1 + x(\lambda-1)}\, dx \\
&= [k \log(1 + x(\lambda-1))]_0^1 \\
&= k \log \lambda
\end{aligned} \tag{66}$$

Hence

$$P = \left(\frac{R}{r}\right)^k \tag{67}$$

Next, [51] assumes that the volume involved increases linearly with time $R(t)^3 \equiv J_0 t$. Then we have $P \propto t^{-k/3}$. Hence the probability of no spin-spin resonance decreases as a power law in time, which means that the system thermalises in algebraically long time. This is named a "critical time-crystal" [51]. However, this power-law relaxation was not observed in the experiment [30].

E.2.3 $\alpha < 2d$

Within a volume R^d of the a two-spin system, the probability that there is another two-spin system is $JR^{d-\alpha}$ as above. The number of two-spin systems is then $R^d \cdot JR^{d-\alpha} = JR^{2d-\alpha}$. When $\alpha < 2d$, a pair of two-spin systems will interresonate in the system size limit.

Appendix F MBL - Poisson Level Spacing

In an MBL system, there is no level repulsion, leading to a Poisson / Exponential distribution for energy levels E_n. We show this by assuming that:
1. Means energy levels are independent and uncorrelated
2. Probability density is translation invariant and $\mathbb{P}(E_n \in [E, E+\delta E]) = \rho\delta E$ occur randomly with rate parameter ρ.

Let $E_1 > E_0$ be two adjacent energy levels, and we seek the probability of having an energy gap of size $S > 0$. Probability that there is no energy level in $[E_0, E_0 + S]$: partition the interval into m segments of length $\frac{S}{m}$, each of which must contain no energy level. As we send $m \to \infty$,

$$\mathbb{P}(\text{No level in}[E_0, E_0 + s]) = \left(1 - \rho\frac{S}{m}\right)^m \to e^{-\rho S} \tag{68}$$

We have $\mathbb{P}(\text{one level in}[E_0 + S, E_0 + S + \delta S]) = \rho\delta S$. Define $s \equiv \rho S$, the expected number of energy levels in $[E, E + S]$, then

$$\mathbb{P}(\text{No level in } [E_0, E_0+s] \text{ and one level in } [E_0+S, E_0+S+\delta S]) = \rho\delta S e^{-\rho S} = e^{-s}\delta s \tag{69}$$

Thus $\mathbb{P}(E_1 - E_0 \in [S, S + \delta S])$ follows the Poisson or Exp(1) distribution for having 0 events with rate s.

F.1 Consecutive Levels Ratio Statistic

We define the Level Statistic as [35]:

$$r = \frac{\min_n\{E_{n+2} - E_{n+1}, E_{n+1} - E_n\}}{\max_n\{E_{n+2} - E_{n+1}, E_{n+1} - E_n\}} \tag{70}$$

Let $S_n = E_{n+1} - E_n$ be the level spacing. Since S_n, S_{n+1} are independently and identically distributed as per Eq 69, we may compute the distribution of r by drawing two samples S_1, S_2. Then either $S_1 \geq S_2$ or vice versa, thus $r = \min\left(\frac{S_1}{S_2}, \frac{S_2}{S_1}\right)$.

$$\begin{aligned}
\mathbb{P}(r \leq x) &= \mathbb{P}(S_1 \leq xS_2 \text{ or } S_2 \leq rS_1) \\
&= 2\int_0^\infty \left(\int_0^{xS_2} \rho e^{-\rho S_1}\, dS_1\right) \rho e^{-\rho S_2}\, dS_2 \\
&= 2\int_0^\infty (1 - e^{-\rho x S_2})\rho e^{-\rho S_2}\, dS_2 \\
&= 2\left(1 - \int_0^\infty \rho e^{-\rho(1+x)S_2}\, dS_2\right) \\
&= 2\left(1 - \frac{1}{1+x}\right) \\
&= \frac{2x}{1+x}
\end{aligned} \tag{71}$$

Thus the probability density is:

$$f(r=x) = \frac{d}{dx}\left(\frac{2x}{1+x}\right) = \frac{2}{(1+x)^2} \tag{72}$$

The expectation value is

$$\mathbb{E}[r] = \int_0^1 \frac{2r}{(1+r)^2}\, dr = 2\ln 2 - 1 = 0.386 \tag{73}$$

If the energy levels are instead the eigenvalues of a random matrix drawn from Gaussian Orthogonal Ensemble (GOE), The mean $\mathbb{E}[r] = 0.536$ for GOE distribution [52], which represent thermal systems. Other settings such as GUE, GSE are also discussed. For further discussion see [53, 54].

Appendix G Other Information

In the transverse field Ising model, a gauge transformation can be done to ensure the couplings are always positive [55]. Hence we only consider the case where $J_i \geq 0, h_i^x \geq 0$.

Example: For $N = 4$, if $J_1 = +1, J_2 = -1, J_3 = +1$, domain walls are energetically favoured at $D_2 = Z_2 Z_3$. Then consider

$$\begin{aligned} \tilde{H} &= (X_3 X_4)^\dagger H (X_3 X_4) \\ &= -\left[J_1 Z_1 Z_2 + J_2 Z_2 (-Z_3) + J_3 (-Z_3)(-Z_4)\right] - \sum_{i=1}^{4} h_i^x X_i \end{aligned} \tag{74}$$

This allows us to effectively flip the sign of J_2. Similarly we can ensure h_i^x are positive by conjugating H with the corresponding Z_i.

Appendix H Notation

X, Y, Z: pauli matrices with eigenvalues ± 1.

Incommensurate: irrational ratios

J_{ij}: coupling between physical bits

$h_i^{x,z}$: perturbation on p-bits

B_i: equivalent to h_i but for l-bits

K_{ij}: equivalent to J_{ij} but for l-bits

I_i: local integral of motion / logical bit

S_i^z: psuedo-spin. Used this to avoid confusion with τ.

$\tilde{D}, \tilde{P}, \tilde{H}, \tilde{U}$: tilde represents the dressed version after perturbation.

$\tau_i^z = V Z_i V^\dagger$: dressed spin operators

$|\{z_i\}\rangle, |\alpha\rangle$: a product state, but in general not an eigenstate.

$|\psi\rangle$: eigenstates of driven system

$\equiv$: definition